Proc. NIPR Symp. Antarct. Meteorites, 5, 74–119, 1992

MINERALOGY AND PETROLOGY OF AN UNUSUAL BELGICA-7904 CARBONACEOUS CHONDRITE: GENETIC RELATIONSHIPS AMONG THE COMPONENTS

Makoto KIMURA[1] and Yukio IKEDA[1]

[1] *Department of Earth Sciences, Ibaraki University, 1–1, Bunkyo 2-chome, Mito 310*

Abstract: Belgica-7904 (B-7904) carbonaceous chondrite consists of abundant chondrules, various clasts, isolated minerals, and a dehydrated phyllosilicate matrix. Chondrules are divided into magnesian and ferroan types. Magnesian type has forsterite phenocryst, often with pyroxene, plagioclase, and unusual Cr-rich ovoid, which set in a dehydrated phyllosilicate groundmass. Kamacite is abundantly included in the forsterite phenocrysts, and is rarely associated with schreibersite. Ferroan type consists mainly of ferroan olivine phenocryst and dehydrated phyllosilicate groundmass with phosphate, instead of schreibersite in magnesian type. Clasts in B-7904 are classified into seven types. These include matrix-like clasts, phyllosilicate-rich clasts, hortonolite-rich clasts (aggregates of ferroan olivine and opaque minerals), Mn-rich olivine-bearing clasts containing schreibersite, Mn-rich forsterite, and Mn-rich chromite, forsterite-spinel clasts like amoeboid olivine inclusions (AOI's) in C3 chondrites, kamacite-rich clasts, and sulfide-rich clasts consistsing of troilite, pentlandite, taenite, and Co-rich metal. Mineralogical study suggests that magnesian chondrules, phyllosilicate-rich clasts, and Mn-rich olivine-bearing clasts formed under reducing conditions, whereas ferroan chondrules, hortonolite-rich clasts, and the matrix originated under oxidizing conditions. Thus, the components of B-7904 originated in different reservoirs with contrasting fO_2 and fS_2 in the solar nebula, and were later mixed. Glass inclusion in chondrules, which occur in olivine phenocrysts and dehydrated phyllosilicate groundmasses, contains CaO, whereas phyllosilicates in the groundmass are nearly free from CaO. Thus, CaO was mainly lost from these chondrules during hydrous alteration, although some CaO remains as abundant phosphate in ferroan chondrules. All of the CaO lost from the chondrules and clasts appears to have been concentrated in the matrix as Ca-carbonates. The oxidation reaction to form magnetite and magnesiowüstite from kamacite also took place in a magnesian chondrule at about 660 K and 10^{-36} bars oxygen partial pressure, which is much higher than an oxygen partial pressure (10^{-43} bars) of the canonical solar gas with a total gas pressure of 10^{-4} bars at 600 K. This suggests that magnesian chondrules were oxidized by a nebular gas of non-solar composition, probably after mixing with ferroan chondrules. All phyllosilicates in B-7904 were dehydrated by intense heating, and the unequilibrated mineral assemblages and the magmatic temperatures retained in some of the chondrules suggest that the heating took place for a short duration, probably by shock heating.

1. Introduction

A carbonaceous chondrite B-7904 has been extensively studied for mineralogy and petrology (KOJIMA *et al.*, 1984; SKIRIUS *et al.*, 1986; AKAI, 1988; PRINZ *et al.*, 1989; TOMEOKA, 1990; BISCHOFF and METZLER, 1991), and chemistry (KALLEMEYN, 1988; PAUL and LIPSCHUTZ, 1989). Although their results generally suggest that B-7904 resembles CM chondrites, B-7904 has an oxygen isotopic feature similar to CI chondrites (MAYEDA *et al.*, 1987). However, the presence of abundant chondrules distinguishes B-7904 from normal CI chondrites. On the other hand, B-7904 has also unusual characteristic features which are not observed in normal CM chondrites; large chondrules occur abundantly (BISCHOFF and METZLER, 1991), PCP and magnetite are absent and rare, respectively (TOMEOKA, 1990), some volatile trace elements are depleted (PAUL and LIPSCHUTZ, 1989), and phyllosilicates in chondrules and matrix have been dehydrated (KOJIMA *et al.*, 1984), which is supported by the observation that its water content is very low when compared with other CM chondrites (HARAMURA *et al.*, 1983). Thus, KOJIMA *et al.* (1984), AKAI (1988), and TOMEOKA (1990) suggested that B-7904 experienced thermal metamorphism on the parent body, after the formation of phyllosilicates. All these characteristic features show that B-7904 is an unusual carbonaceous chondrite different from normal CI and CM chondrites.

As part of the consortium study on three Antarctic unusual carbonaceous chondrites (B-7904, Yamato(Y)-82161 and -86720), we have carried out a detailed mineralogical and petrological study of B-7904 using a scanning electron microscope (SEM). In contrast with Y-82161, -86720, and other CM chondrites, B-7904 has abundant primary components which have experienced little hydrous alteration. The purposes of this study are (1) classification of components based on texture and mineralogy, (2) detailed petrography of the components, (3) clarification of the genetic relationhsips among the components, and (4) clarification of the reheating process of the components in B-7904.

2. Samples and Experimental Method

Four polished thin sections of B-7904: 92-1, 92-2, 92-3, and 94-2, were available for this study. They were studied previously by several consortium members. Each thin section, except for 92-3, covered only a half to one-third of the whole area. The compositions of the constituent minerals were measured with a JEOL 733 type electron-probe microanalyzer (EPMA). The accelerating voltage and beam current were 15 kV and 3 to 10 nA, respectively. The Bence-Albee correction method was used for the analysis of silicates and oxides, and the ZAF method was used for the metals, sulfides, some phosphates, and magnesiowüstite. The oxygen contents of magnesiowüstite and some magnetites were measured using the same method as that in IKEDA (1991), for magnesiowüstite in Y-82162 chondrite. A special X-ray peak deconvolution program was applied to correct for X-ray overlaps of K_β line of Ti on the K_α of V for analyses of chromite and other phases. The peak intensities of Co K_α and the background for Fe-Ni metal were carefully measured in order to

Table 1. The components of B-7904.

Chondrule	Magnesian Ferroan	
Silicate-rich clast	Matrix-like clast	Pyroxene-bearing Pyroxene-free
	Hortonolite-rich clast	Taenite-troilite-bearing Kamacite-phosphate-bearing
	Phyllosilicate-rich clast	Opaque mineral-poor Opaque mineral-rich
	Mn-rich olivine-bearing clast	
	Forsterite-spinel clast	Forsterite-rich Spinel-rich
Opaque mineral-rich clast	Kamacite-rich clast Sulfide-rich clast	
Isolated minerals	Silicate, Oxide, Phosphate, Carbonate, Metal, Sulfide	
Matrix		

Table 2. Mineral assemblages

	Chondrules		Silicate-rich Clasts			
	Magnesian	Ferroan	Matrix-like		Hortonolite-rich	
			Pyoxene -bearing	Pyroxene -free	Taenite- troilite -bearing	Kamacite- phosphate -bearing
Olivine	+	+		+	+	+
Ca-poor Pyroxene	+		+			
Ca-rich Pyroxene	+					
Plagioclase	+					
Glass	+	+				
Phyllosilicate	+	+	+	+	+	+
Spinel	+					
Chromite	+	+	+			
Eskolaite	+					
Magnesiowüstite	+					
Magnetite	+					
Phosphate		+	+	+	+	+
Carbonate						
Kamacite	+					+
Co-rich metal						
Taenite	+	+	+	+	+	
Schreibersite	+					
Troilite	+	+	+	+	+	+
Pentlandite	+	+	+			

avoid the overlapping of Fe and Co. All analyses, including those for the fine-grained dehydrated phyllosilicates in the matrix, were carried out with a focused beam of the EPMA.

3. Petrography

3.1. Classification of the components

The components of B-7904 are classified into chondrules, clasts, isolated minerals, and matrix based on their texture and mineralogy (Table 1). Chondrules are defined as fragmental to spherical objects which show textural evidence of crystallization from a melt. Clasts are mineral clusters which do not show any textural evidence of crystallization from a melt, and have clear boundaries with the matrix. Five types of silicate-rich clasts and two types of opaque mineral-rich clasts were distinguished. Isolated minerals consist of mineral grains, larger than a few microns, which occur in the matrix. The matrix consists of very fine-grained dehydrated phyllosilicates which fill the interstices among the other components. The constituent minerals of these components are summarized in Table 2. All the phyllosilicates in B-7904 are dehydrated and are converted to secondary olivine as shown by transmission electron microscope (TEM) study (AKAI, 1988). Nevertheless, they preserve the textures

of the components in B-7904.

Silicate-rich Clasts					Opaque mineral-rich Clasts		Isolated minerals	Matrix
Phyllosilicate-rich		Mn-rich olivine-bearing	Forsterite-spinel		Kamacite -rich	Sulfide -rich		
Opaque mineral -poor	Opaque mineral -rich		Forsterite -rich	Spinel -rich				
+	+	+	+	+			+	
							+	
+	+	+	+	+	+		+	+
			+	+				
+		+					+	
+								
					+			
+							+	
							+	
+					+		+	
						+		
+	+			+		+	+	+
+		+						
+	+	+	+	+	+	+	+	+
+						+	+	

and chemistry of the original phyllosilicates on a micron-sized scale. In this study we shall call them phyllosilicates for convenience.

The distribution and abundances of the components are heterogeneous in the thin sections of B-7904, although this is partly due to the small areas and poor condition of the thin sections. BISCHOFF and METZLER (1991) reported an ilmenite-bearing Al-rich inclusion which may have been a Ca-Al-rich inclusion (CAI). Although we studied the same three thin sections as theirs (92-1, 92-2, and 94-2), we did not find this inclusion and a large chondrule mentioned in their paper. These components may have been missed before we got these sections.

3.2. Chondrule

Chondrules, 70–2400 microns in size, are abundant in B-7904. Most of chondrules have a porphyritic texture (Fig. 1–1), and only a few barred-olivine chondrules were found. Chondrules are divided into magnesian and ferroan types, on the basis of the compositions of predominant olivine. The compositional range of olivine in the magnesian chondrules is Fo_{90-99} with a predominant composition of Fo_{98-99}, whereas that in the ferroan chondrules is Fo_{34-99} with a predominant composition of Fo_{46-86}. MCSWEEN (1977) and MCSWEEN *et al.* (1983) devised a classification for chondrules in carbonaceous chondrites, based on texture and mineralogy; Type I chondrule has a granular texture and olivines of Fo_{90-100}, and Type II has a porphyritic or barred texture and olivine of Fo_{50-85}. We found a barred-olivine chondrule containing olivine of Fo_{99}, which can not be classified into type I and II chondrules. Therefore, here we do not use the criteria proposed by MCSWEEN (1977) and MCSWEEN *et al.* (1983).

Magnesian chondrules are more abundant, and ferroan type is less than about one-fourth of magnesian type in abundance. Chondrules of both types consist mainly of olivine phenocryst and groundmass, but the accessory minerals are different in each type as shown in Table 2. Olivine in chondrules usually has euhedral to subhedral forms, and experienced little hydrous alteration. Most of groundmasses in chondrules have been replaced by phyllosilicates. The size distribution of the chondrules is not different between the two types. Most of chondrules are fragmental in shap.

3.2.1. Magnesian chondrule

Large magnesian chondrules, larger than about 500 microns, always show a core-mantle structure (Fig. 1–1), but small chondrules do not have such a structure. The mantle consists mainly of phyllosilicates showing a coarse-grained platy texture, although the core consists of primary anhydrous minerals with phyllosilicates showing a fine-grained massive texture (Fig. 1–2). A few large chondrules have euhedral to subhedral coarse-grained Ca-poor pyroxene in the cores (Fig. 1–3), whereas the mantle of chondrules has irregularly shaped fine-grained Ca-poor pyroxene as a relic mineral (Fig. 1–4). Ca-rich pyroxenes occur as small phenocrysts in core of a large magnesian chondrule (Fig. 1–3), and as a tiny inclusion in a forsterite phenocryst (Fig. 1–5). A few large chondrules often have plagioclase as well as pyroxene in their cores (Fig. 1–6), and another large chondrule has glassy groundmass in the core (Fig. 1–4). Spherical glass inclusions, up to 10 microns in diameter, are

Fig. 1-1. Back-scattered electron (BSE) image of a large magnesian chondrule, showing a core (C)-mantle (M) structure. Dust rim (DR) with abundant opaque minerals surrounds this chondrule. Width of 800 microns.

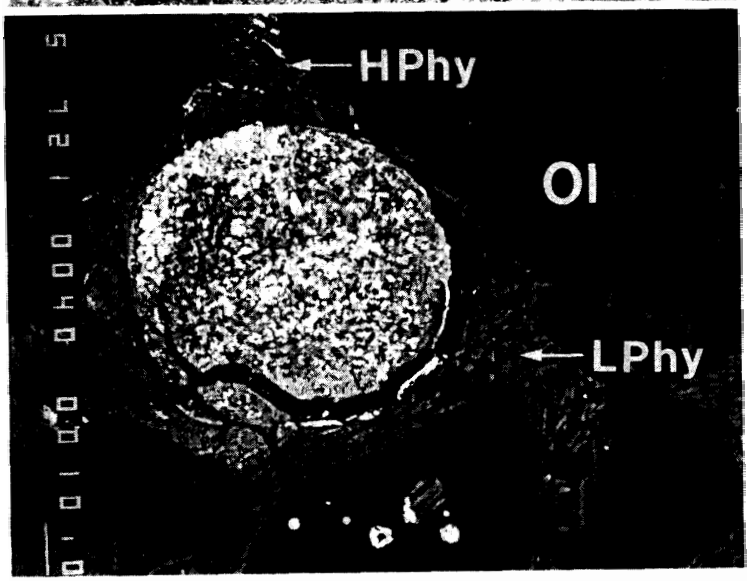

Fig. 1-2. BSE image of a detail of the magnesian chondrule of Fig. 1–2. High-Al phyllosilicate (HPhy) shows a massive texture, whereas low-Al phyllosilicate (LPhy) platy texture. A spherical Cr-rich ovoid occurs with the phyllosilicate and olivine (Ol). Width of 140 microns.

Fig. 1-3. BSE image of the core of a large magnesian chondrule, including coarse-grained olivine (Ol) and enstatite (En), fine-grained diopside (Di), and phyllosilicate (Phy). Glass (Gl) occurs in intimate association with phyllosilicate. Width of 160 microns.

Fig. 1-4. Fine-grained enstatite (En) and olivine phenocryst (Ol) among phyllosilicate groundmass (Phy) in a mantle of a large magnesian chondrule. Note the difference in morphology and grain size of enstatite between core (Fig. 1–3) and mantle of chondrule. BSE image. Width of 210 microns.

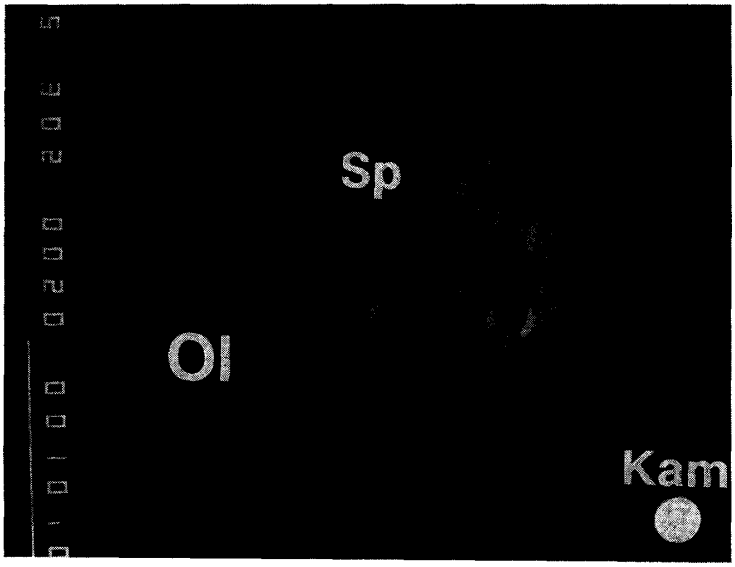

Fig. 1-5. BSE image of a glass (Gl)-spinel (Sp)-fassitic pyroxene (Fas) inclusion in an olivine phenocryst in a magnesian chondrule. Width of 30 microns.

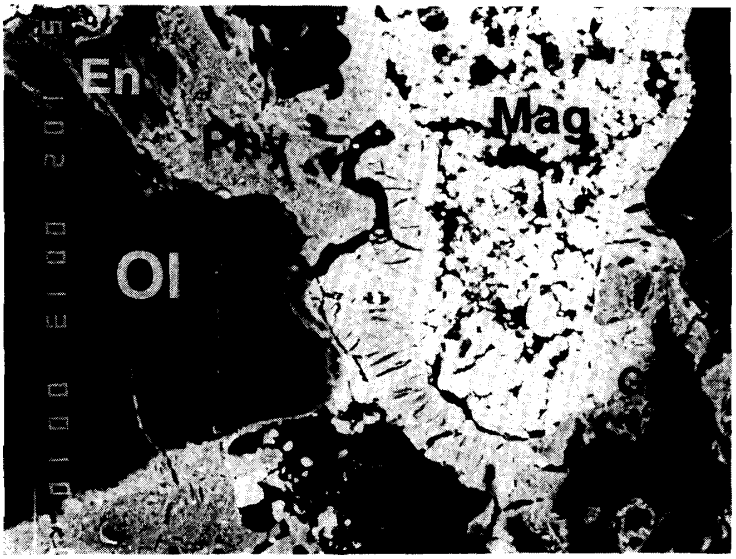

Fig. 1-6. A core of a large magnesian chondrule, consisting of olivine (Ol), enstatite (En), plagioclase (Pl), phyllosilicate (Phy), and magnetite (Mag). A plagioclase grain has a SiO_2-rich glass inclusion (Gl). BSE image. Width of 100 microns.

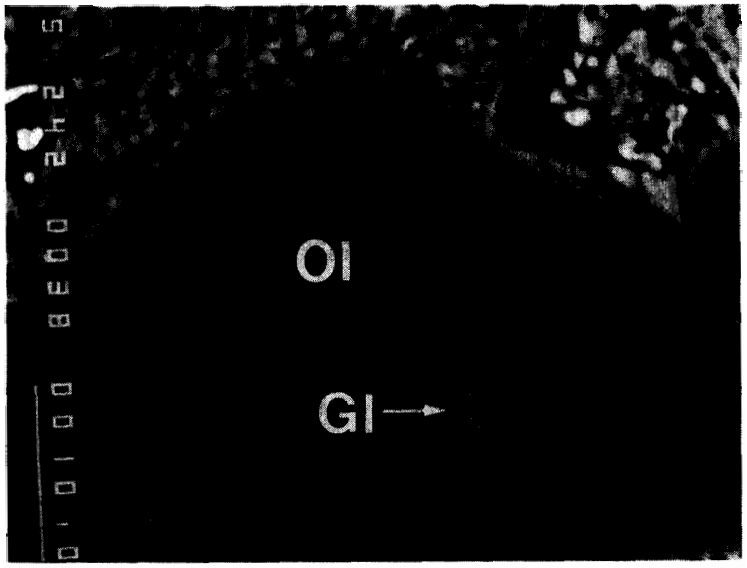

Fig. 1-7. BSE image of a glass inclusion in an olivine phenocryst (Ol) in a magnesian chondrule. Width of 40 microns.

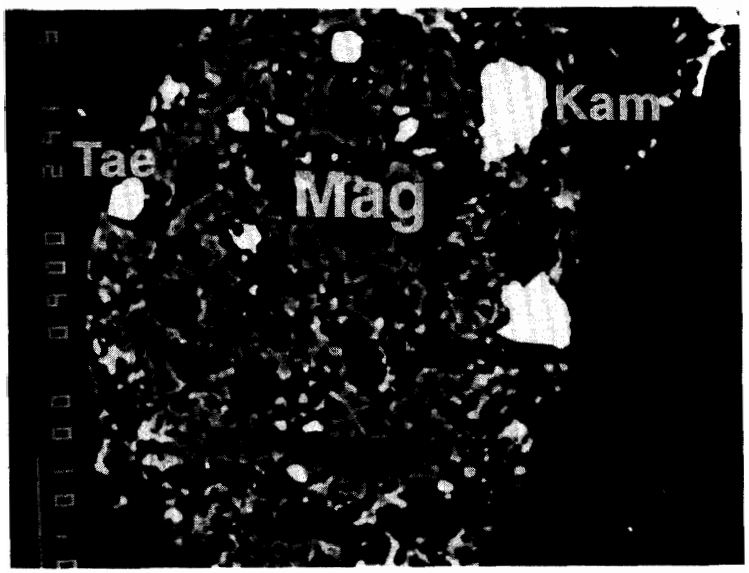

Fig. 1-8. BSE image of a magnetite (Mag)-kamacite (Kam)-taenite (Tae) aggregate in a large magnesian chondrule. This aggregate is the same as magnetite in Fig. 1–6. Note that magnetite seems to be porous. Width of 60 microns.

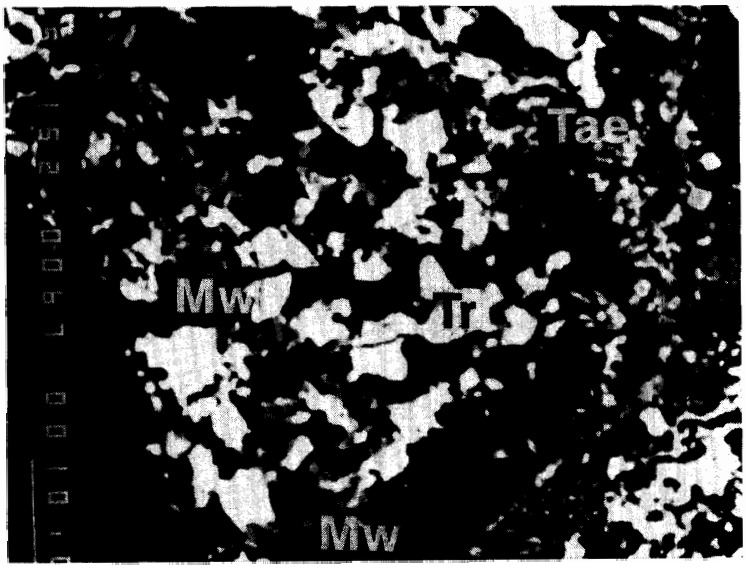

Fig. 1-9. BSE image of a magnesiowüstite (Mw)-troilite (Tr)-taenite (Tae) aggregate in a large magnesian chondrule. Magnesiowüstite grains are very small in size, up to 5 microns. This aggregate occurs near a magnetite-kamacite-taenite aggregate (Fig. 1–8) in the same chondrule. Width of 110 microns.

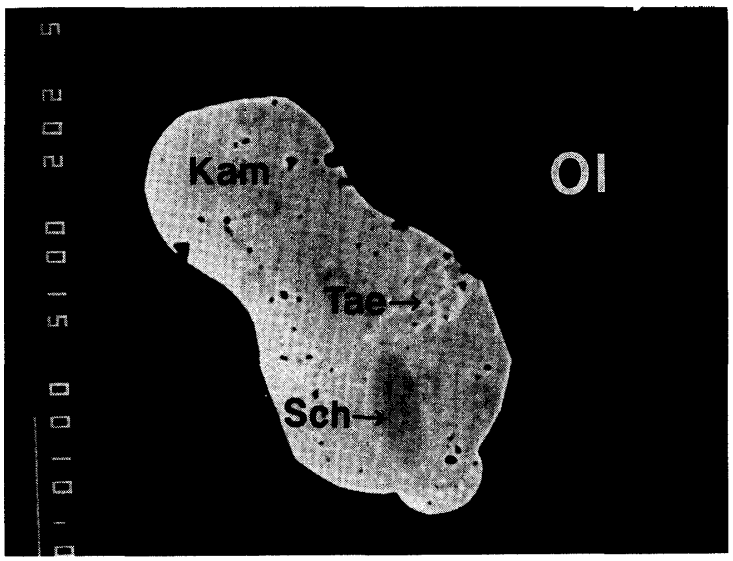

Fig. 1-10. BSE image of a kamacite inclusion (Kam) in association with taenite (Tae) and schreibersite (Sch), in a forsterite phenocryst in a magnesian chondrule. Width of 50 microns.

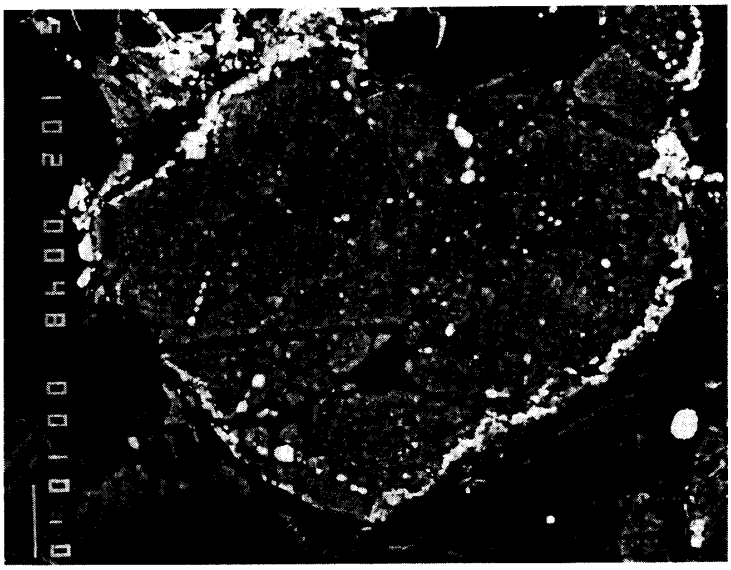

Fig. 1-11. Chromite (Chr) occurs in the peripheral parts of Cr-rich ovoid in a magnesian chondrule. BSE image. Chromite in magnesian chondrules always occurs in Cr-rich ovoids as irregular-shaped grain. Width of 130 microns.

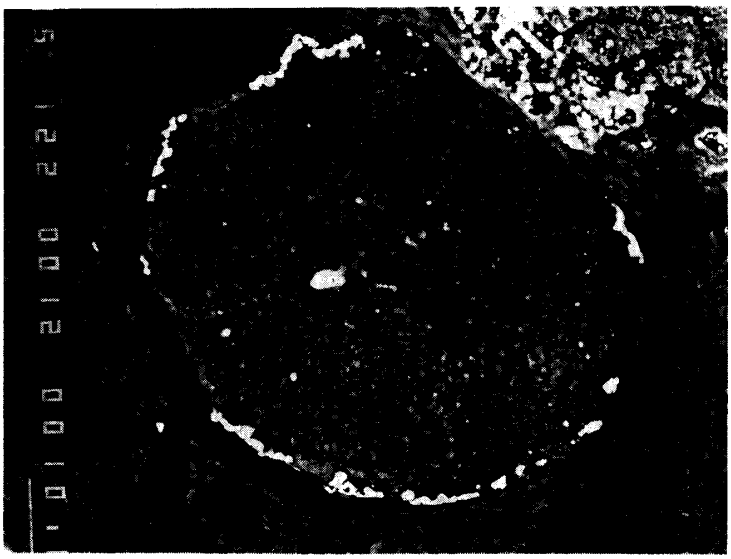

Fig. 1-12. Eskolaite (Esk) occurring in the peripheral parts of Cr-rich ovoid in a magnesian chondrule. A troilite grain (Tr) is included in the central part of this Cr-rich ovoid. BSE image. Width of 130 microns.

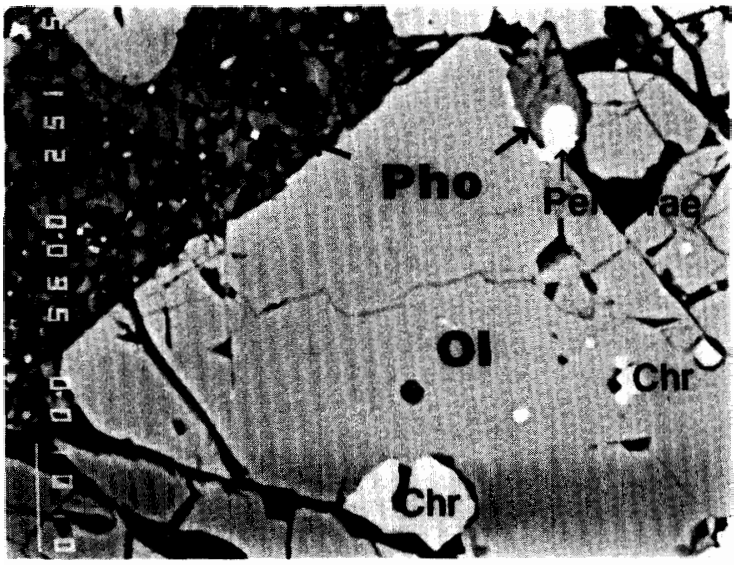

Fig. 1-13. BSE image of the detail of a ferroan chondrule. Olivine phenocryst (Ol) has chromite inclusions (Chr). Phosphate (Pho), and aggregate of pentlandite and taenite (Pen+Tae) occur between olivine grains. Groundmass also has phosphate (gray) in addition to phyllosilicate (dark). Width of 110 microns.

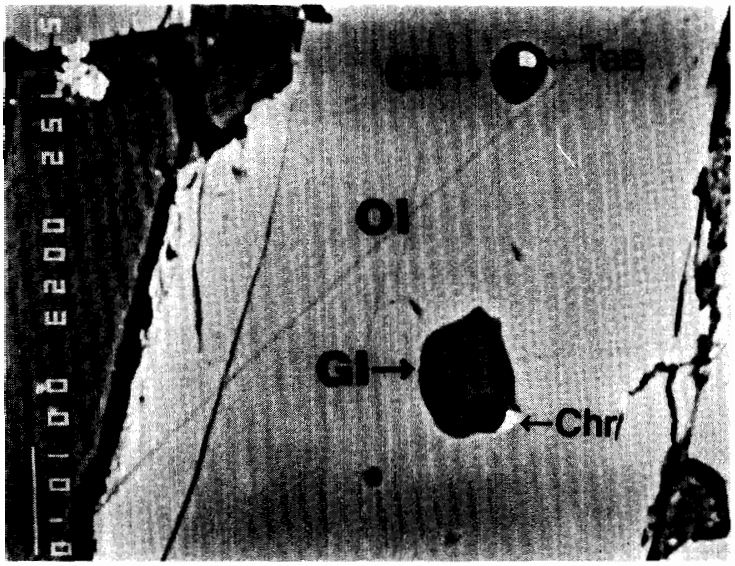

Fig. 1-14. BSE image of glass inclusions (Gl) in intimate association with taenite (Tae) and chromite (Chr) in an olivine phenocryst (Ol) in a ferroan chondrule. Glass inclusions in ferroan chondrules are usually accompanied by a spherical hole (bubble). Width of 110 microns.

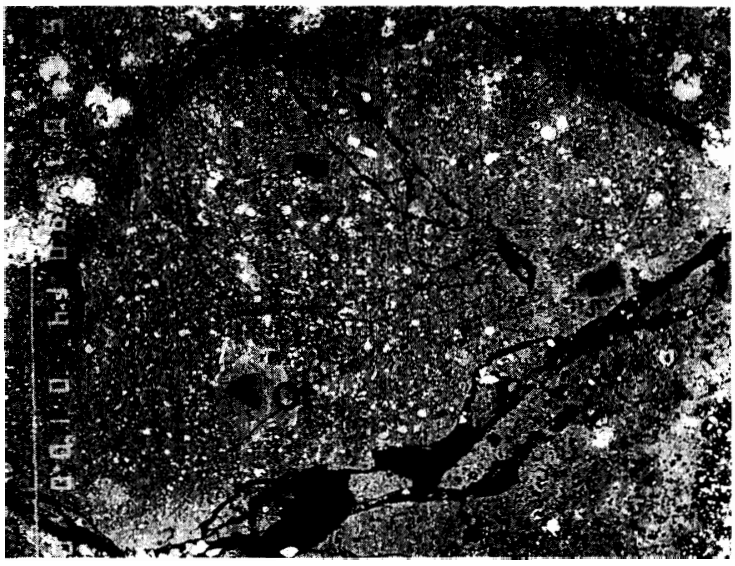

Fig. 1-15. BSE image of a matrix-like clast. Forsteritic olivine fragments (Ol) occur in the fine-grained phyllosilicate matrix. Width of 250 microns.

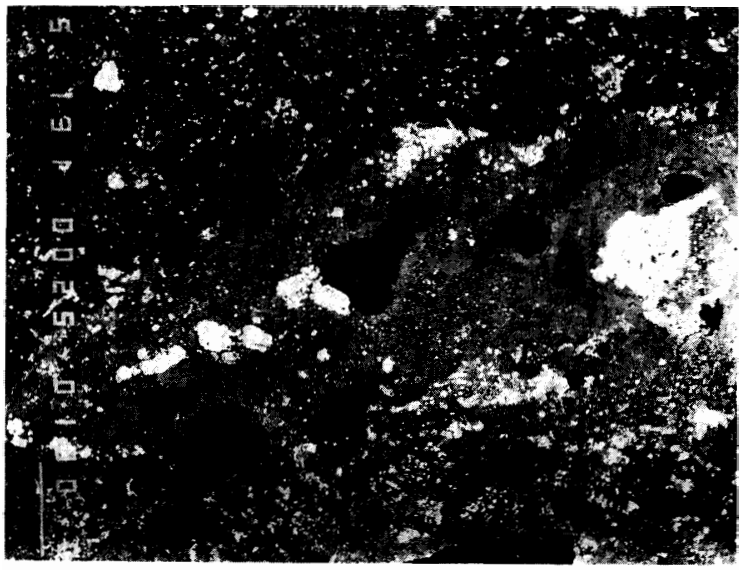

Fig. 1-16. BSE image of a matrix-like clast including pyroxene fragments. Several pyroxene fragments (Px), and aggregates of troilite and pentlandite (bright) occur in the phyllosilicate. Width of 800 microns.

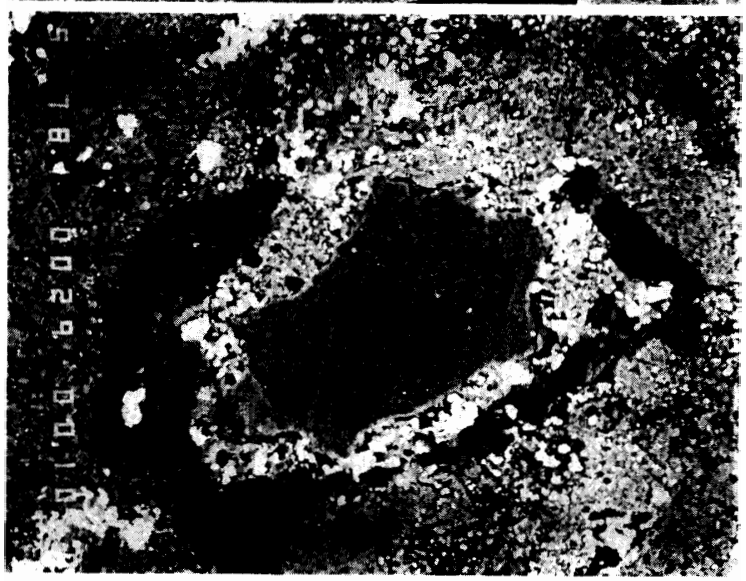

Fig. 1-17. BSE image of a phyllosilicate-rich clast (Phy) surrounded by forsteritic olivine (Ol). Troilite and chromite (bright) occur abundantly in the interstices between olivine and phyllosilicate. Width of 140 microns.

Fig. 1-18. BSE image of a phyllosilicate-rich clast. Halos in phyllosilicate surrounding cavities are enriched in Fe (bright areas), whereas other phyllosilicates (dark areas) are magnesian. Irregular-shaped troilite often occurs within cavities. Width of 210 microns.

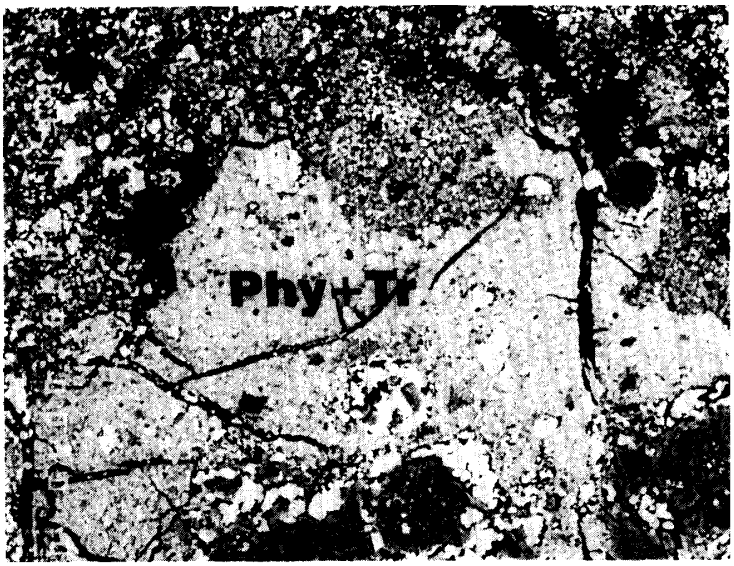

Fig. 1-19. A phyllosilicate-rich clast, consisting of phyllosilicates with abundant fine-grained troilite (Phy+Tr). BSE image. Width of 140 microns.

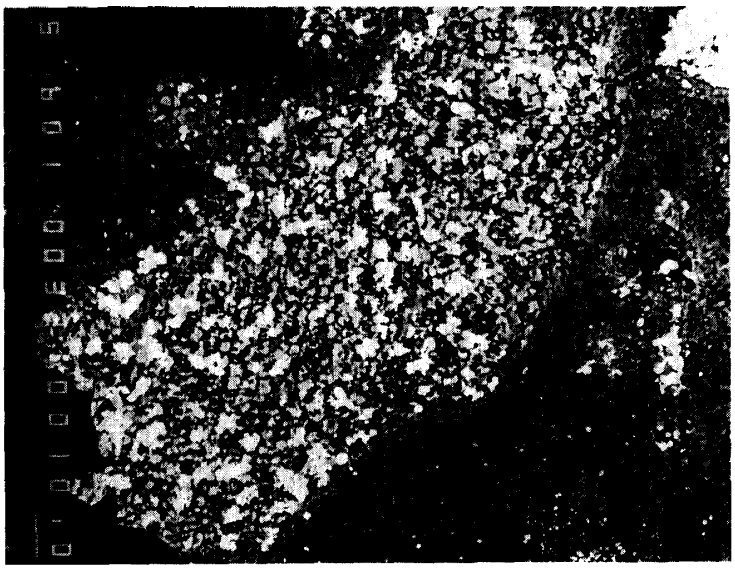

Fig. 1-20. BSE image of a hortonolite-rich clast, consisting of fine-grained taenite and troilite (bright), olivine (gray), and phosphate (gray). Width of 160 microns.

Fig. 1-21. BSE image of a hortonolite-rich clast, consisting of olivine (Ol), kamacite (Kam), and phosphate (Pho). There are abundant cavities, especially around kamacite, in this clast. A phosphate-rich rim surrounds this clast. Width of 170 microns.

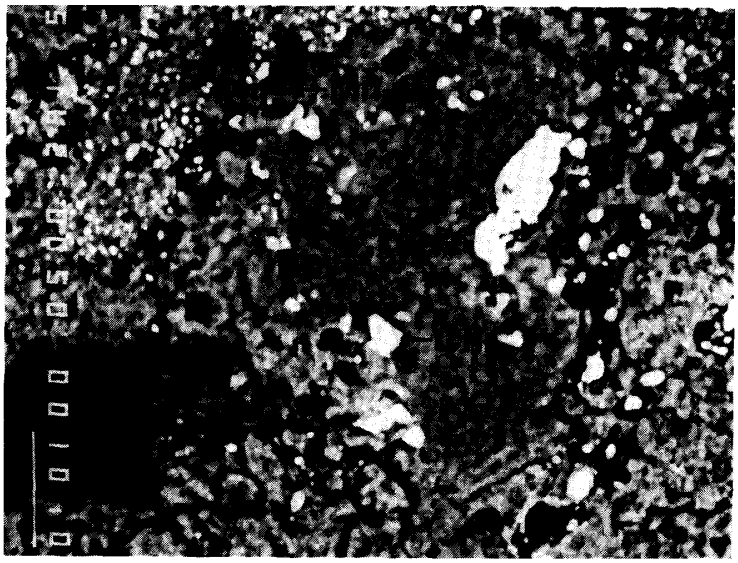

Fig. 1-22. BSE image of a Mn-rich olivine-bearing clast, consisting of MnO-bearing olivines (Mn-Ol), MnO-rich chromites (Chr), schreibersite (Sch), taenite (Tae), and phyllosilicate (Phy). Width of 60 microns.

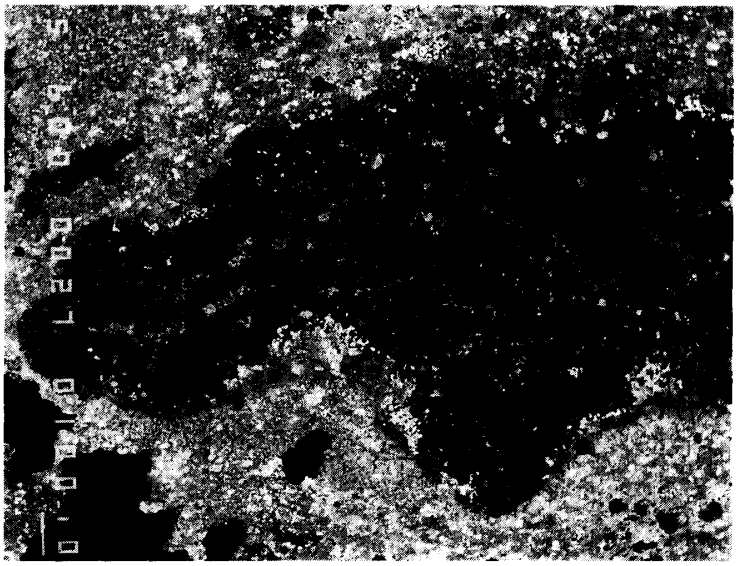

Fig. 1-23. BSE image of forsterite-rich subtype of forsterite-spinel clasts consisting mainly of forsteritic olivine with interstitial phyllosilicates. Width of 1900 microns.

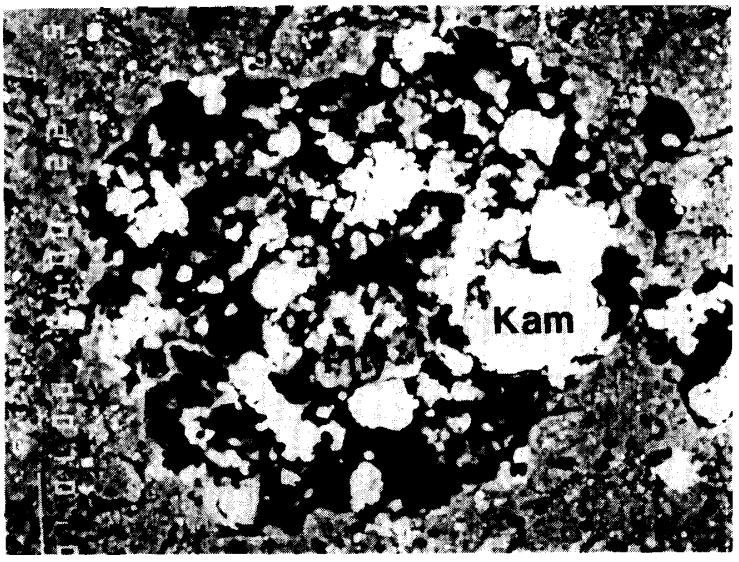

Fig. 1-24. BSE image of a kamacite-rich clast, consisting mainly of kamacite (Kam) with a small amount of phyllosilicate (Phy). There are many cavities in the kamacite-rich clast, which seem to be plucked areas which were clasts originally. Width of 130 microns.

Fig. 1-25. A sulfide-rich clast consisting of troilite (Tr), pentlandite (Pen), taenite (Tae), and Co-rich metal (CoMet). Sulfide-rich clasts always have irregular-shaped taenite and often Co-rich metal. BSE image. Width of 50 microns.

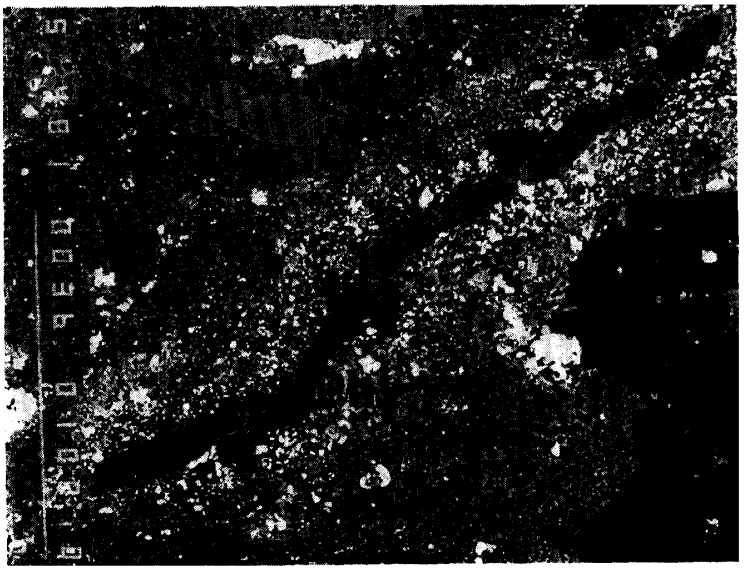

Fig. 1-26. An elongated vein-like phyllosilicate grain (Phy) in the matrix. Such a grain has clearly different texture from the matrix phyllosilicates. BSE image. Width of 210 microns.

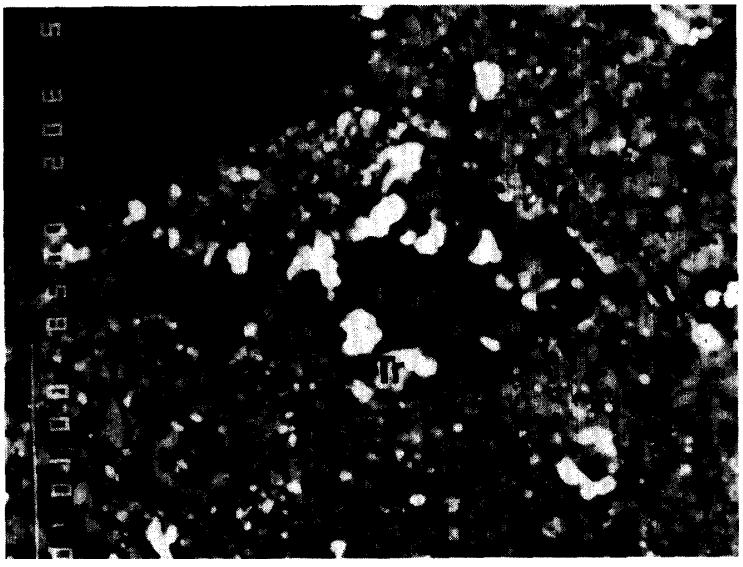

Fig. 1-27. BSE image of a Ca-carbonate grain (Carb) with troilite (Tr) in the matrix. Only a few Ca-carbonate grains were found in B-7904. Width of 30 microns.

Fig. 1-28. BSE image of an olivine phenocryst in a ferroan chondrule. This olivine grain has remarkable zoning, from a forsteritic core (Fo_{95}) to a fayalitic rim (Fo_{45}). Width of 170 microns. Note that the forsteritic core seems to be a relic.

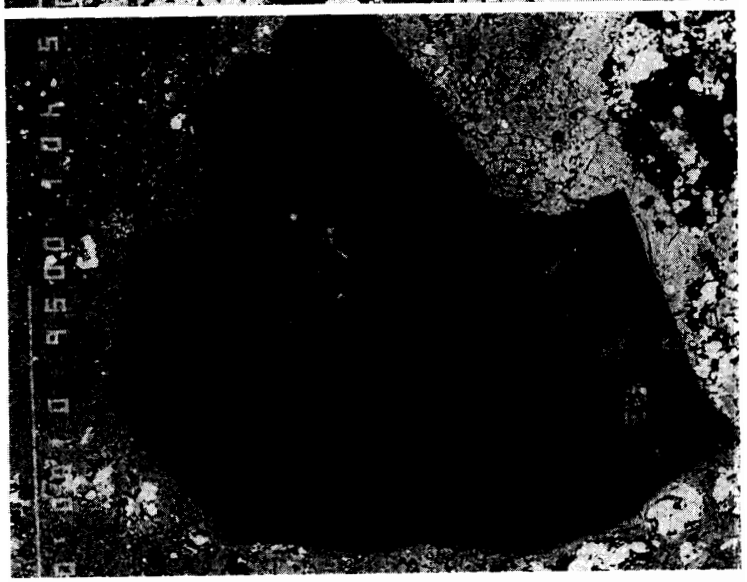

Fig. 1-29. BSE image of an isolated mineral of forsterite in the matrix. Note that this grain has no ferroan rim in its peripheral parts. Width of 250 microns.

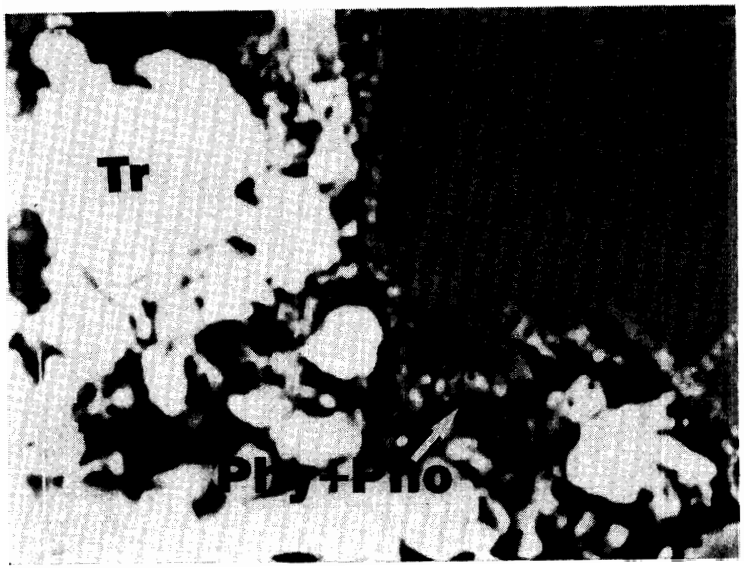

Fig. 1-30. BSE image of an olivine phenocryst (Ol) and troilite (Tr) in a ferroan chondrule. The interstices are filled by phyllosilicate and phosphate (Phy+Pho). Very fine-grained wollastonite and sulfide (bright blebs) occur along the peripheral parts of the olivine phenocryst. The olivine has reverse zoning only in the peripheral part (dark). Width of 30 microns.

commonly encountered within olivine phenocrysts (Fig. 1–7). They are not devitrified. PRINZ *et al.* (1989) found rare micron-sized grains of zircon in forsterite.

A magnesian chondrule includes an aggregate of magnetite-kamacite-taenite assemblage (Fig. 1–8). Magnesiowüstite, up to 5 microns in size, occurs within another aggregate of troilite-taenite near the magnetite-kamacite-taenite aggregate in the same chondrule (Fig. 1–9). Kamacite occurs as tiny spherical to ellipsoidal inclusions in forsterite phenocrysts (Fig. 1–10), and it rarely coexists with schreibersite. The groundmass of magnesian chondrules contains taenite, troilite, and often pentlandite. Groundmass phyllosilicates in a few magnesian chondrules have bright halos around irregular-shaped troilite grains.

Magnesian chondrules often have unusual spherical to ellipsoidal inclusions within the groundmass (Fig. 1–2), and forsterite phenocrysts rarely have such inclusions. They are 20–200 microns in size, and brown to black in color. These brown inclusions consist mainly of phyllosilicates, whereas the black inclusions have abundant opaque minerals such as troilite, taenite, and schreibersite. Fine-grained chromite and eskolaite, up to 3 microns, also occur as irregular-shaped grains in and around the brown and black inclusions (Figs. 1–11 and 1–12). The brown inclusions have been described as egg-shaped particles by BISCHOFF and METZLER (1991), and as brown balls in CR2 chondrites by PRINZ (personal comm., 1991). We shall call them Cr-rich ovoids, because they are rich in Cr_2O_3 as noted below.

Magnesian chondrules, especially large ones, have well-developed fine-grained dust rims, and they consist of phyllosilicates and opaque minerals such as troilite, taenite and pentlandite (Fig. 1–1).

3.2.2. Ferroan chondrule

Ferroan chondrule contains no pyroxene and Cr-rich ovoid. The groundmass consists mainly of phyllosilicates, but sometimes fine-grained Ca-phosphates abundantly occur in the groundmass, as already noticed by PRINZ *et al.* (1989). The phosphate, up to 5 microns in size, occurs in contact with phenocrystic olivine (Fig. 1–13). Spherical glass inclusions, up to 10 microns in diameter, are also encountered in the olivine phenocrysts (Fig. 1–14), and they often associate with taenite, troilite, and chromite. Most of them are accompanied by a spherical bubble. Euhedral chromite, up to 20 microns in size, usually occurs in the groundmass, as shown by JOHNSON and PRINZ (1991). The groundmass also contains taenite, troilite, and often pentlandite.

Dust rims are often observed around ferroan chondrules, and fine-grained opaque minerals in the rims are sparse, compared with those around magnesian chondrules. However, large chondrules often have sulfide-metal rims.

3.3. Clast

B-7904 has seven types of clasts, 30–1800 microns in size. Most clasts are smaller than 100 microns in size and irregular in shape. Some large clasts have distinct dust rims similar to those around chondrules. Cr-rich ovoids have not been found in any of these clasts.

3.3.1. Matrix-like clast

Matrix-like clasts consists of phyllosilicates with fine-grained fragments of olivine,

phosphate, chromite, troilite, and taenite (Fig. 1–15). The phyllosilicates are fine-grained, as in the matrix, and the same accessory minerals occur in matrix-like clasts as well as in the matrix. Thus, these clasts resemble the matrix, although they have clear outlines against it. One matrix-like clast has Ca-poor pyroxene instead of olivine (Fig. 1–16).

3.3.2. Phyllosilicate-rich clast

They are predominant among all clast types, and consist of phyllosilicates with minor olivine, chromite, phosphate, schreibersite, taenite, and troilite. Phyllosilicate-rich clasts show a wide variation in texture and mineralogy, and they are divided into opaque mineral-poor and -rich subtypes. Opaque mineral-poor subtype is predominant. A few clasts of opaque mineral-poor subtype are surrounded by troilite and taenite rims, and some by forsterite rims (Fig. 1–17). Back-scattered electron (BSE) images reveal that a few clasts of opaque mineral-poor subtype include porous bright halo around irregular-shaped troilite grains (Fig. 1–18). The opaque mineral-rich subtype is black in color, and comprises abundant fine-grained troilite and often taenite in association with phyllosilicate (Fig. 1–19). A few clasts of this subtype have abundant spherical taenite and troilite grains.

3.3.3. Hortonolite-rich clast

They are classified into taenite-troilite-bearing and kamacite-phosphate-bearing subtypes. Only one clast of each subtype has been found. Phyllosilicate occurs in a negligible amount. The taenite-troilite-bearing subtype is an aggregate of hortonolitic olivine, fine-grained taenite, and troilite with minor phosphate (Fig. 1–20). All of the constituent minerals are very small, up to 5 microns. The kamacite-phosphate-bearing subtype consists mainly of hortonolitic olivine, fine-grained phosphate, and kamacite (Fig. 1–21). A thin phosphate rim, about 2–5 microns in width, surrounds the clast.

3.3.4. Mn-rich olivine-bearing clast

Two Mn-rich olivine-bearing clasts were found. They consist mainly of phyllosilicates with minor amounts of forsterite, chromite, schreibersite, taenite, and troilite (Fig. 1–22). Forsterite and chromite are rich in MnO, as noted below. Schreibersite occurs in association with taenite.

3.3.5. Forsterite-spinel clast

This clast type consists of subhedral to anhedral spinel and forsterite, 1–15 microns in size, with a minor amount of phyllosilicates, and is divided into forsterite-rich (Fig. 1–23) and spinel-rich subtypes. TOMEOKA (1990) also found a spinel-rich clast (called spinel aggregate in his paper). The interstices between forsterite or spinel grains are filled by phyllosilicates, although some forsterite-spinel clasts are nearly free from phyllosilicate. Troilite and taenite often occur as inclusions in the interstitial phyllosilicates.

3.3.6. Kamacite-rich clast

Kamacite-rich clasts consist mainly of kamacite with variable amounts of troilite, magnetite and phyllosilicates (Fig. 1–24). Fine-grained phyllosilicates, smaller than 5 microns in size, occur sparsely between kamacite grains. Kamacite-rich clasts always have abundant cavities, up to about 10 microns.

3.3.7. Sulfide-rich clast

Sulfide-rich clasts consist of troilite, pentlandite, and taenite, often associated with Co-rich and Ni-poor metal (Fig. 1–25). Troilite is predominant. The mineral assemblage is similar to that found in sulfide-metal rims around chondrules. No other silicate or oxide minerals occur within them.

3.4. Isolated mineral

Many kinds of isolated fragmental minerals, 2 to 120 microns in size, occur in the matrix. These are olivine, Ca-poor pyroxene, phyllosilicates, chromite, phosphate, carbonate, kamacite, taenite, troilite, and pentlandite. Some phyllosilicate grains show a coarse-grained platy texture similar to that in the chondrules. One vein-like isolated phyllosilicate grain is 300 microns long and 10 microns wide (Fig. 1–26). Only a few fine-grained carbonate grains occur in the matrix (Fig. 1–27), which are mixed with troilites. Fine-grained Ca-phosphates, smaller than 5 microns in size, occur abundantly in the matrix, as also noted by MATSUNAMI *et al.* (1989).

3.5. Matrix and dust rim

Matrix in B-7904 consists of fine-grained phyllosilicate, smaller than 1 micron in size. Very fine-grained opaque minerals, up to 1 micron, are abundantly distributed in the matrix. Qualitative analyses of the matrix show that it contains Fe, Ni, and S, suggesting that the matrix includes troilite, taenite, and/or probably pentlandite. The abundances of opaque minerals in the matrix are higher than those in the chondrules.

Distinct dust rims surround large chondrules and clasts. Although the textures of the dust rims are very similar to those of the matrix, a larger amount of opaque minerals (troilite, taenite, and pentlandite) characterize the dust rims (Fig. 1–1). The dust rims also include silicate and phosphate fragments.

4. Mineralogy

4.1. Olivine

Olivine occurs in chondrules and silicate-rich clasts, and as isolated minerals. Table 3a gives representative compositions of olivines in different components. The compositions of olivine depend upon its occurrences. Magnesian chondrules have forsteritic olivines (Fo_{90-99}), and do not have zoning, except for narrow 1–2 micron wide FeO-enriched rims. Some fine-grained olivine in the groundmass of magnesian chondrules is slightly enriched in FeO (Fo_{90-95}). Olivine in magnesian chondrules contains 0.0–0.9 wt% Cr_2O_3, 0.0–0.2% NiO, 0.0–0.8% MnO, and 0.0–0.7% CaO.

Olivine in ferroan chondrules has a wider compositional range (Fo_{34-99}). Most are zoned from magnesian cores to ferroan rims. Some olivine phenocrysts in ferroan chondrules have distinct magnesian core (Fo_{95}), in contrast to their ferroan rims (Fo_{45}) (Fig. 1–28). Olivine in ferroan chondrules contains 0.0–0.6 wt% Cr_2O_3, 0.0–0.3% NiO, 0.0–0.9% MnO, and 0.0–0.7% CaO.

The forsterite-spinel, phyllosilicate-rich, Mn-rich olivine-beraing, and matrix-like

Table 3a. Representative

Phase	Occurrence	SiO_2	TiO_2	Al_2O_3	Cr_2O_3	FeO	NiO
Olivine	Magnesian chondrule	41.65	0.01	0.00	0.16	0.34	0.05
Olivine	Magnesian chondrule	41.08	0.02	0.00	0.53	4.06	0.06
Olivine	Ferroan chondrule	33.50	0.02	0.04	0.15	42.44	0.15
Olivine	Ferroan chondrule	39.94	0.04	0.05	0.33	10.07	0.00
Olivine	Phyllosilicate-rich clast	41.85	0.05	0.00	0.34	0.72	0.00
Olvine	Hortonolite-rich clast	32.81	0.00	0.00	0.21	46.20	0.17
Olivine	Mn-rich olivine-bearing clast	40.51	0.03	0.58	0.20	5.76	0.21
Olivine	Forsterite-rich clast	41.58	0.06	0.00	0.32	0.18	0.00
Olivine	Isolated mineral	35.74	0.02	0.04	0.42	31.23	0.05
Olivine	Isolated mineral	41.98	0.02	0.00	0.39	0.38	0.00
Olivine[1)]	Ferroan chondrule	42.43	0.06	0.00	0.89	23.55	0.23
Pyroxene	Magnesian chondrule	51.08	0.84	6.63	0.92	0.41	0.00
Pyroxene	Magnesian chondrule	43.58	2.13	18.55	0.35	0.14	0.00
Pyroxene	Magnesian chondrule	58.51	0.17	0.59	0.49	0.41	0.00
Pyroxene	Matrix-like clast	52.34	0.03	0.04	0.67	25.80	0.06
Pyroxene	Isolated mineral	52.35	0.00	0.03	0.65	22.41	0.11
Plagioclase	Magnesian chondrule	44.65	0.07	35.05	0.03	0.30	0.13
Glass	Magnesian chondrule	56.76	0.30	19.63	0.35	0.17	0.03
Glass	Magnesian chondrule	89.86	0.32	6.36	0.02	0.57	0.00
Glass	Ferroan chondrule	59.15	0.64	16.67	0.24	2.68	0.11

[1)] Analytical data of an olivine contaminated by wollastonite in a ferroan chondrule.

clasts also have forsteritic olivines (Fo_{95-99}), but olivine in hortonolite-rich clast type is ferroan (Fo_{38-46}). Olivine in Mn-rich olivine-bearing clasts is rich in MnO (1.2–2.7%), although that in other clast types is poor in MnO (<1%). Isolated olivine grain in the dust rims and matrix shows wide variations in composition (Fo_{35-99}), which overlaps with those in chondrules and clasts (Fo_{34-99}). Although isolated forsterite grains in the matrix often have very thin FeO-rich rims, about 1–2 microns in width, like those in magnesian chondrules, some isolated forsterite grains in the matrix do not have FeO-rich rims (Fig. 1–29).

As shown in Figs. 2a and 2b, olivines in magnesian chondrules and in some silicate-rich clasts have MnO/FeO ratios higher than that of the CI chondrites (ANDERS and GREVESSE, 1989). On the other hand, olivines in ferroan chondrules and hortonolite-rich clasts have MnO/FeO ratios similar to that of the CI chondrites. The MnO/FeO ratios of isolated olivine in the matrix overlap with those in the magnesian and ferroan chondrules (Fig. 2c).

Rims of some olivine phenocrysts, smaller than 5 microns in width, in a few ferroan chondrules have a reverse zoning; for example Fo_{55} in the outermost rim and Fo_{47} in the inner area. These rims are enriched in CaO, up to 16.0%, and seem to include a very fine-grained CaO-bearing phase, lower than 1 micron (Fig. 1–30). The groundmass surrounding these olivines consists of phyllosilicates with a large amount of Ca-phosphates. However, the CaO-rich rims of olivine phenocrysts do not contain P_2O_5, suggesting that another CaO-bearing phase exists in the rims. We plotted the compositions of the rims in Fig. 3 in order to identify the tiny

compositions of silicate phases.

MnO	MgO	CaO	Na_2O	K_2O	P_2O_5	Total	Fo	En	Wo	An	Ab
0.11	56.28	0.37	0.00	0.00	0.01	98.98	0.997				
0.31	53.46	0.15	0.00	0.00	0.01	99.68	0.959				
0.57	20.98	0.50	0.00	0.00	0.09	98.44	0.469				
0.12	48.92	0.17	0.00	0.00	0.02	99.66	0.896				
0.17	55.75	0.15	0.00	0.00	0.04	99.07	0.993				
0.54	17.60	0.35	0.00	0.00	0.00	97.88	0.404				
2.20	47.74	0.17	0.09	0.04	0.03	97.56	0.937				
0.15	56.85	0.06	0.00	0.00	0.00	99.20	0.999				
0.30	30.63	0.18	0.00	0.04	0.11	98.76	0.636				
0.35	56.60	0.11	0.00	0.00	0.07	99.90	0.996				
0.48	13.30	16.01	0.00	0.02	0.08	97.05					
0.12	20.23	19.64	0.00	0.00	0.13	100.00		0.585	0.408		
0.00	11.31	24.06	0.00	0.00	0.00	100.12		0.394	0.603		
0.05	38.70	0.48	0.00	0.00	0.02	99.42		0.985	0.009		
0.29	19.73	0.30	0.00	0.03	0.00	99.29		0.574	0.006		
0.36	22.24	0.04	0.00	0.00	0.05	98.24		0.639	0.001		
0.03	0.70	18.81	0.13	0.00	0.09	99.99				0.987	0.013
0.00	4.80	16.20	0.15	0.05	0.14	98.58					
0.00	0.01	2.92	0.07	0.00	0.00	100.13					
0.00	2.10	12.63	3.51	0.23	1.33	99.29					

CaO-bearing phase. Only wollastonite fits this chemical trend. Diopside and monticellite in Fig. 3, and other CaO-bearing phases such as åkermanite, rankinite, and merwinite do not fit the trend. Thus, this CaO-bearing phase must be wollastonite. Qualitative analysis shows that some fine-grained sulfide is also included in the rims.

4.2. Pyroxene

Ca-poor pyroxene occurs in large magnesian chondrules and a pyroxene-bearing matrix-like clast, and as an isolated mineral. Ca-poor pyroxene in chondrules is magnesian ($En_{83-99}Fs_{0-5}Wo_{0-14}$), and contains 0.1–0.9 wt% TiO_2 ,0.3–4.1% Al_2O_3, 0.4–1.3% Cr_2O_3 and 0.0–0.3% MnO (Table 3a). Some may be pigeonite, as suggested by the high content of wollastonite molecule. A few pyroxene grains are slightly enriched in FeO, and occur as tiny grains in the chondrule groundmass. Isolated Ca-poor pyroxene in the matrix and in a matrix-like clast are ferroan ($En_{52-73}Fs_{27-47}Wo_{0-1}$), and this shows the chemical heterogeneity in Mg/Mg+Fe ratio of these pyroxene grains. The ferroan pyroxenes contain 0.0–0.1% TiO_2, 0.0–0.3% Al_2O_3, 0.5–0.9% Cr_2O_3, and 0.1–0.4% MnO.

Ca-rich pyroxenes in magnesian chondrules are $En_{64-82}Fs_{0-3}Wo_{35-46}$, and contain variable amounts of minor elements, 0.3–2.0% TiO_2, 0.8–8.6% Al_2O_3, 0.4–1.7% Cr_2O_3, and 0.0–0.7% MnO. The contents of Na_2O and V_2O_3 are below the detection limit. A Ca-rich pyroxene grain, which occurs in association with spinel in an olivine phenocryst (Fig. 1–5), is an Al-Ti-rich fassitic pyroxene (TiO_2 2.1% and Al_2O_3 18.6%).

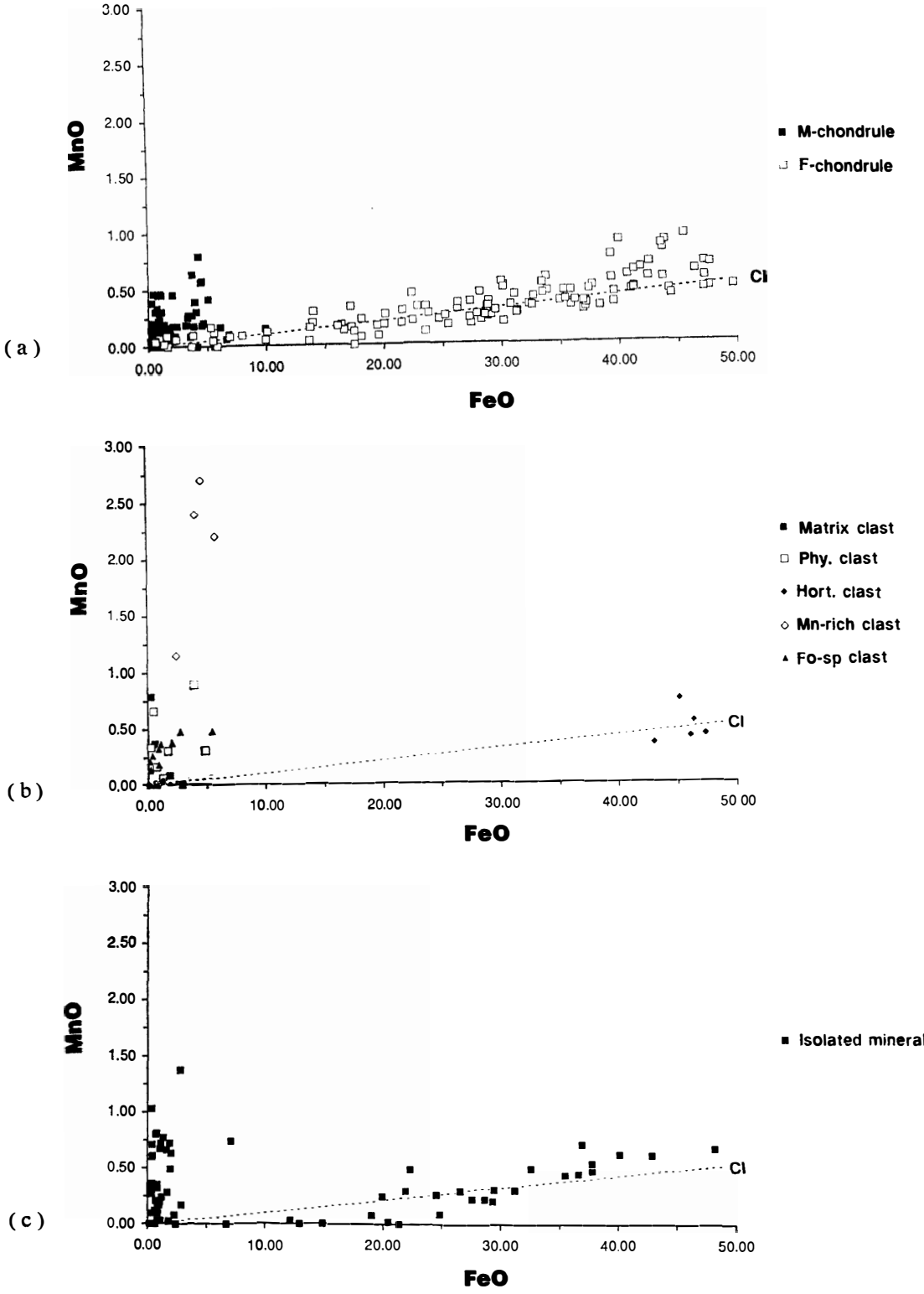

Fig. 2. FeO-MnO (wt%) plot for olivines in (a) magnesian (M) and ferroan (F) chondrules, (b) matrix-like (Matrix), phyllosilicate-rich (Phy), hortonolite-rich (Hort), Mn-rich olivine bearing (Mn-rich), and forsterite-spinel (Fo-sp) clasts, and (c) isolated minerals in the matrix. CI line shows the MnO/FeO ratio of average CI chondrite after ANDERS *and* GREVESSE *(1989).*

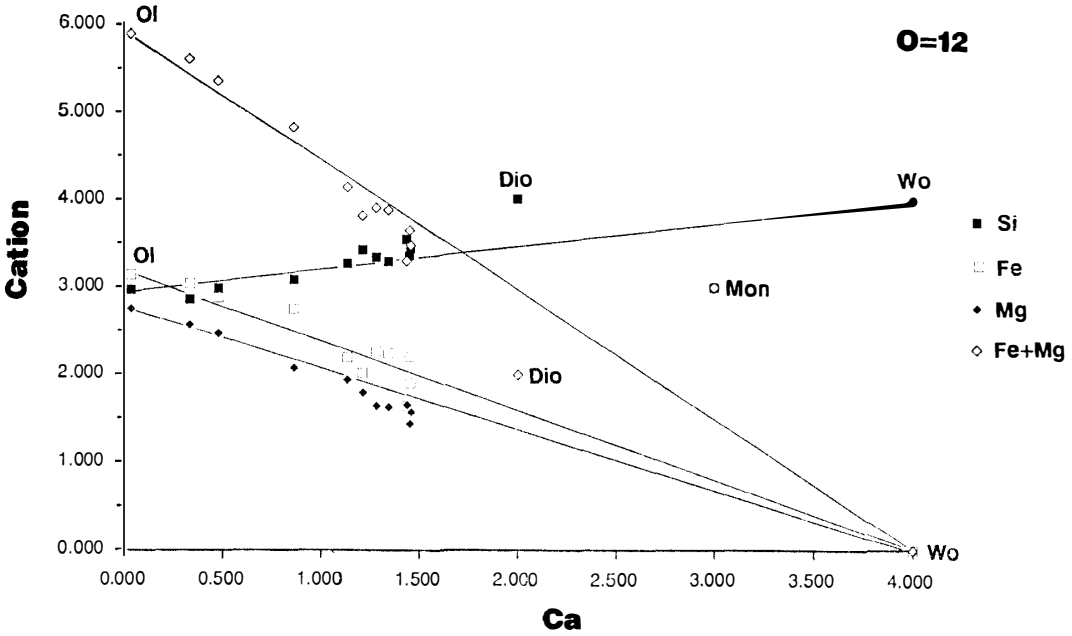

Fig. 3. The atomic compositions of the Ca-rich peripheral rim of an olivine phenocryst in a ferroan chondrule in a diagram of Ca vs. Si, Fe, Mg, and Fe+Mg cations normalized by oxygen=12. Olivine (Ol) in contact with the Ca-rich portion is also plotted. The regression lines indicate that they are mixtures of olivine and wollastonite. Other CaO-bearing minerals such as diopside (Dio) and monticellite (Mon) are not end member phase.

4.3. Plagioclase

Plagioclase occurs only in the cores of a few large magnesian chondrules (Fig. 1–6). They always show irregular shapes, and are anorthitic in composition, An_{90-99}. The K_2O content is below the detection limit.

4.4. Phyllosilicate

Phyllosilicates occur in most of the components. Table 3b gives representative compositions of phyllosilicates in each component. IKEDA *et al.* (1991) classified the phyllosilicates in B-7904 chondrules into high-Al magnesian, high-Al ferroan, and low-Al magnesian types. The boundary between high-Al and low-Al is 6.5 wt% Al_2O_3, and that between magnesian and ferroan is a molar MgO/MgO+FeO ratio of 0.5. This classification is adopted in this paper.

4.4.1. Phyllosilicate in chondrules

The compositions of the phyllosilicates in B-7904 chondrules are mainly distributed between the serpentine (chlorite) and Na-Al-talc lines in Fig. 4. Figure 5 shows the contents of Al_2O_3 and Na_2O+K_2O, and most of them are distributed along the line A-B-C in the figure.

Low-Al magnesian phyllosilicate occurs in small magnesian and ferroan chondrules and in the mantles of large magnesian chondrules. They typically have a coarse-grained play texture (Fig. 1–2). On the other hand, high-Al magnesian phyllosilicate occurs only in the central portions of large magnesian and ferroan chondrules, and have a fine-grained massive texture. The high-Al ferroan type occurs along

Table 3b. Representative compositions of silicate phases (phyllosilicates).

Occurrence	Type	SiO_2	TiO_2	Al_2O_3	Cr_2O_3	FeO	NiO	MnO	MgO	CaO	Na_2O	K_2O	P_2O_5	Total
Magnesian chondrule	HA, ferr	30.37	0.14	20.95	0.15	27.83	0.20	0.29	14.94	0.59	1.61	0.13	0.42	97.84
Magnesian chondrule	HA, mag	42.83	0.12	8.10	1.63	9.71	0.00	0.04	24.45	0.13	1.61	0.31	0.10	89.02
Magnesian chondrule	HA, mag	33.59	0.52	20.54	0.60	17.15	0.09	0.22	19.78	0.29	1.82	0.26	0.62	95.54
Magnesian chondrule	LA, ferr	30.34	0.72	5.43	2.00	32.33	0.74	0.12	16.07	0.16	0.00	0.14	0.18	88.26
Magnesian chondrule	LA, mag	43.93	0.09	4.86	1.03	14.24	0.08	0.17	23.43	0.09	1.27	0.48	0.08	89.89
Ferroan chondrule	HA, mag	37.12	0.61	14.64	0.01	21.03	0.23	0.24	19.25	0.26	1.63	0.21	0.44	95.70
Ferroan chondrule	LA, mag	39.62	0.17	4.02	0.01	17.57	0.10	0.13	26.55	0.20	1.25	0.26	0.10	90.17
Ferroan chondrule	LA, mag	37.98	0.64	5.75	0.48	15.10	0.48	0.24	24.82	3.14	1.77	0.19	2.63	93.31
Matrix-like clast	LA, mag	38.36	0.06	2.71	0.47	18.01	0.14	0.41	22.90	4.86	0.12	0.05	0.03	88.12
Matrix-like clast	LA, mag	36.54	0.21	6.44	1.35	15.64	0.56	0.42	23.53	2.89	0.64	0.28	1.45	90.15
Phyllosilicate-rich clast	LA, ferr	34.93	0.07	3.09	0.50	37.40	0.17	0.17	19.27	1.41	0.91	0.06	0.39	98.55
Phyllosilicate-rich clast	LA, mag	41.66	0.08	3.46	0.56	22.63	0.48	0.20	23.12	0.79	0.85	0.23	0.10	94.16
Mn-rich olivine-bearing clast	LA, mag	37.38	0.11	2.97	0.45	21.04	0.23	0.26	26.91	0.29	0.75	0.18	0.10	90.67
Forsterite-rich clast	HA, mag	36.60	0.17	12.84	0.31	17.45	0.04	0.17	19.33	0.40	2.10	0.54	0.17	90.25
Spinel-rich clast	LA, mag	44.01	0.09	3.68	0.20	10.69	0.10	0.13	34.03	0.25	0.55	0.19	0.00	93.99
Kamacite-rich clast	LA, ferr	27.24	0.00	2.25	0.27	28.91	0.40	0.13	16.14	14.73	0.20	0.02	0.27	90.67
Isolated mineral	LA, mag	38.71	0.11	3.49	1.49	19.85	0.21	0.37	20.74	1.08	1.22	0.44	0.20	88.01
Matrix	LA, ferr	32.84	0.14	2.43	0.33	33.39	1.04	0.35	16.90	1.30	0.02	0.04	0.03	88.93
Matrix	LA, mag	36.29	0.04	4.15	0.74	26.57	0.15	0.37	18.73	2.79	0.73	0.05	1.39	92.17
Matrix	LA, mag	34.81	0.21	2.69	0.42	22.71	0.97	0.29	18.09	5.62	0.80	0.35	0.08	87.17
Matrix	LA, mag	44.38	0.16	4.88	0.80	17.77	0.78	0.22	22.02	0.24	1.17	0.36	0.14	93.07
Dust rim	LA, mag	37.20	0.06	2.85	0.48	23.63	0.62	0.29	22.83	2.91	0.76	0.21	0.06	91.92
Dust rim	LA, mag	45.03	0.07	4.42	1.06	20.30	0.04	0.29	22.48	0.34	1.08	0.16	0.10	95.38
Cr-rich ovoid[1)]		21.68	2.08	4.77	2.35	42.36	9.14	0.44	8.52	0.14	1.11	0.07	1.20	94.18
Cr-rich ovoid[1)]		32.56	0.09	4.12	4.25	21.62	3.29	0.02	24.49	0.09	1.07	0.19	2.59	94.55

Type; La: Low-AI, HA: High-Al, mag: magnesian, ferr: ferroan.

[1)] Analytical data of Cr-rich ovoids are contaminated by opaque minerals such as chromite, taenite, and troilite.

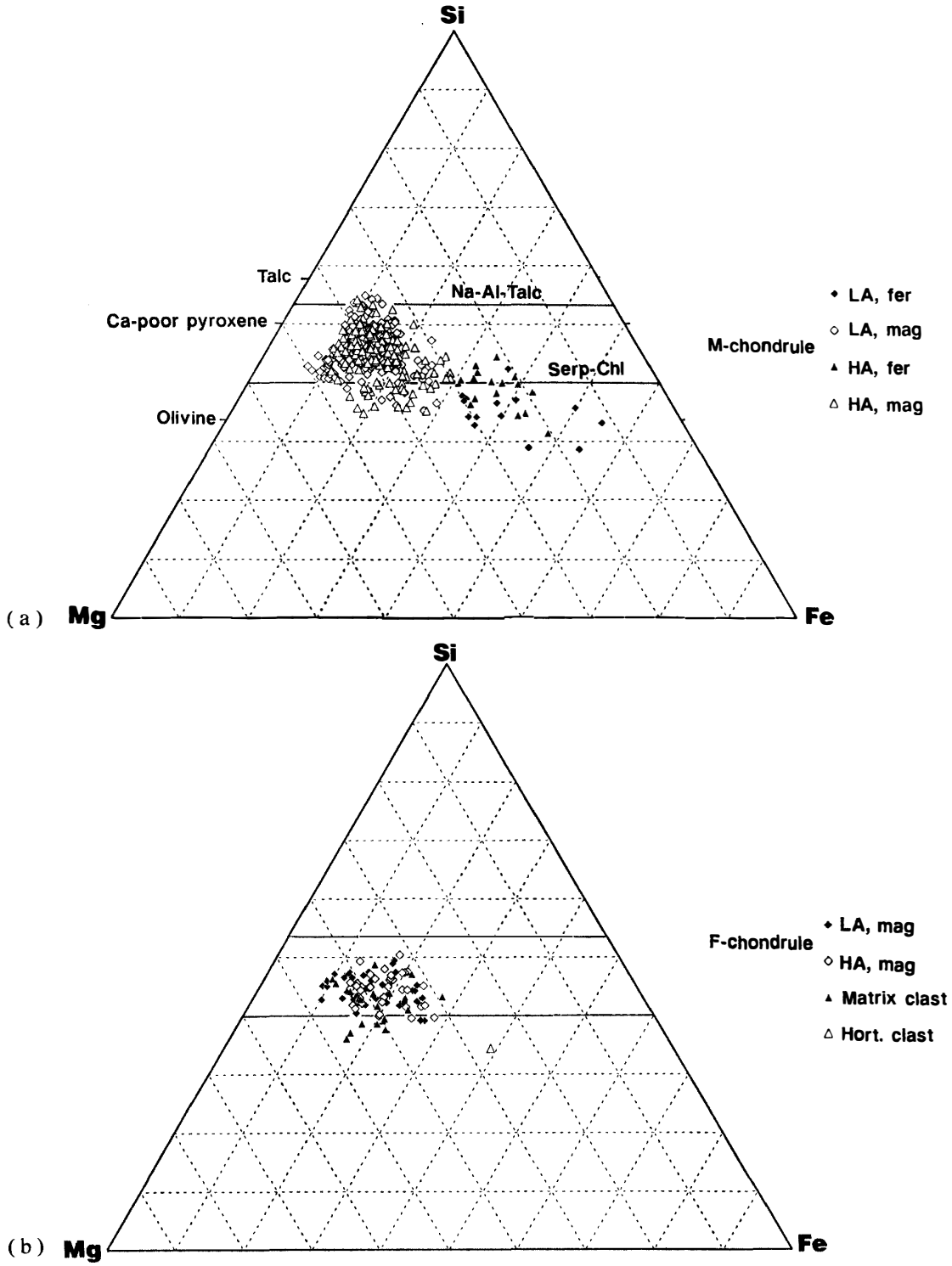

Fig. 4. Atomic Si-Mg-Fe plot of phyllosilicate in (a) magnesian (M) chondrules, (b) ferroan (F) chondrules, matrix-like (Matrix), and hortonolite-rich (Hort) clasts, (c) phyllosilicate-rich (Phy), Mn-rich olivine-bearing (Mn-rich), forsterite-spinel (Fo-sp), and kamacite-rich (Kam) clasts, and (d) the matrix, dust rims, and isolated minerals. LA and HA are low-Al and high-Al phyllosilicates, and mag and fer are magnesian and ferroan phyllosilicates, respectively. Two lines with Na-Al-Talc and Sep-Chl are Mg-Fe solid solutions of Na-Al-talc and serpentine (or chlorite). Analytical data with NiO>1% are excluded in the diagrams, because of the contamination by Fe-Ni metal and pentlandite.

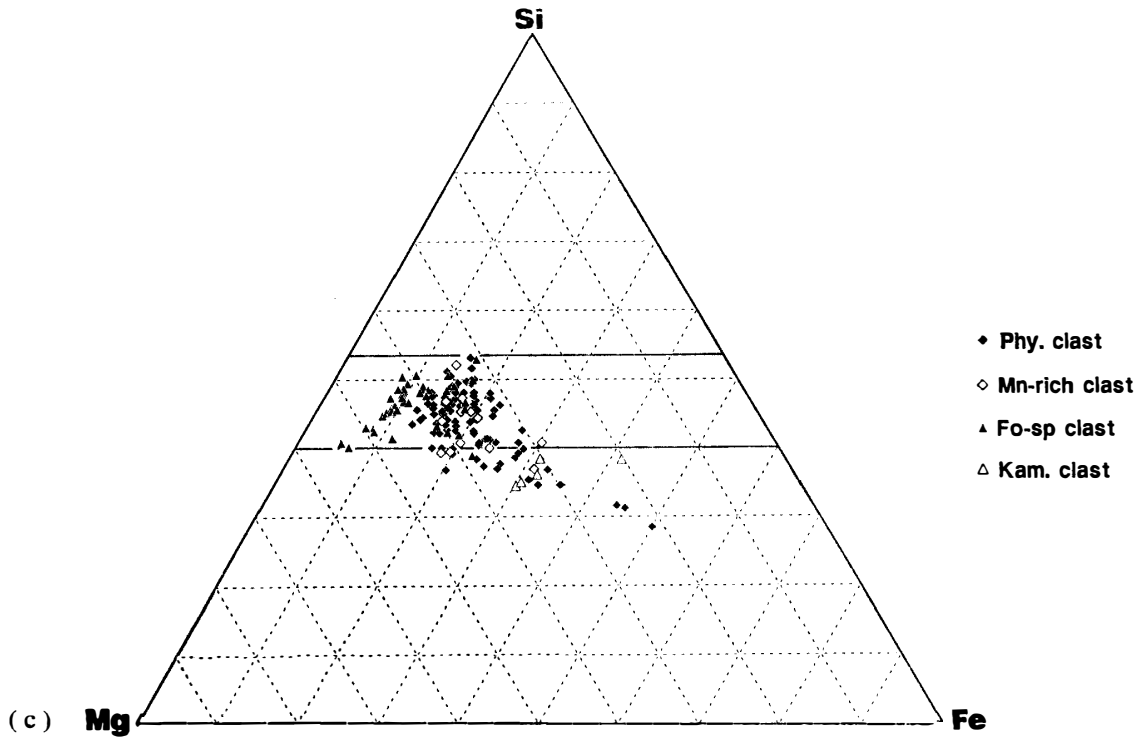

(c)

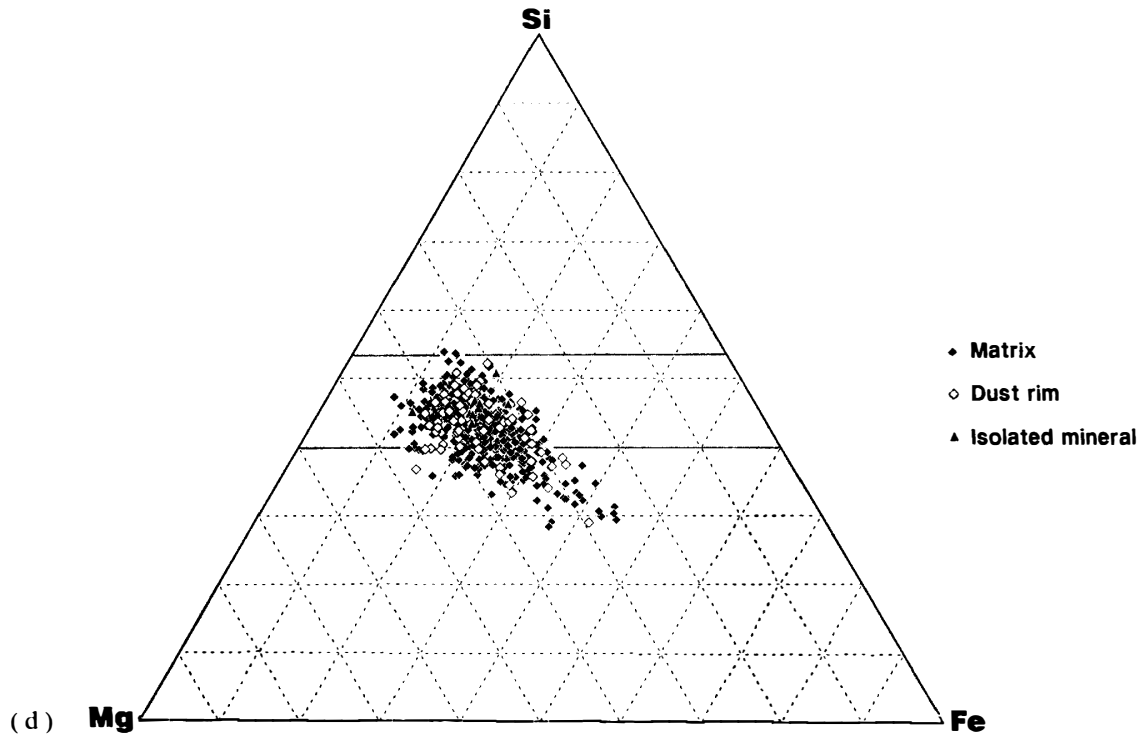

(d)

Fig. 4. (Continued).

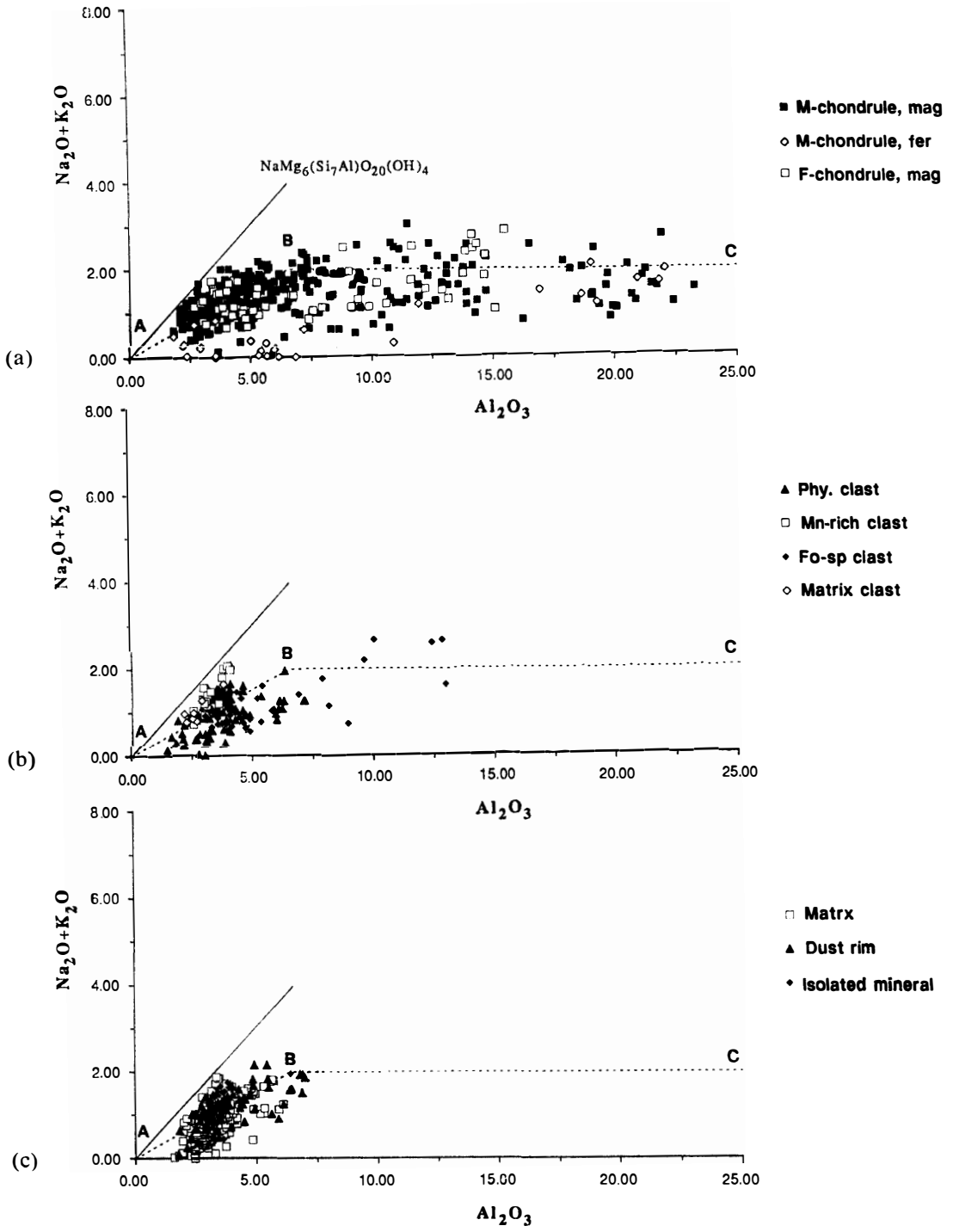

Fig. 5. *Al_2O_3 vs. $Na_2O + K_2O$ (wt%) plot of phyllosilicates in (a) magnesian (M) and ferroan (F) chondrules (mag and fer mean magnesian and ferroan phyllosilicates, respectively), (b) phyllosilicate-rich (Phy), Mn-rich olivine-bearing (Mn-rich), forsterite-spinel (Fo-sp), and matrix-like (Matrix) clasts, and (c) the matrix, dust rims, and isolated minerals. The composition of Na-Al-talc is shown in the diagram for reference. Phyllosilicates containing CaO below 2% are plotted in the figures. A, B, and C show the composition of talc or serpentine, mixed layer mineral between Na-Al-talc Na $(Mg, Fe)_6$ (Si_7Al) O_{20} $(OH)_4$ and serpentine (or chlorite) proposed by* IKEDA *et al. (1991), and a mixture between the mixed layer mineral and aluminous serpentine (or chlorite), respectively. They are connected by a dotted line.*

with opaque minerals (mostly troilite) in the cores of some large magnesian chondrules. Low-Al ferroan type occurs in the cores of large magnesian chondrules with coarse-grained irregular-shaped troilites. They are depleted in Na_2O and K_2O (lower than 0.2%), and plot along the serpentine (chlorite) solid solution line in Fig. 4. They may be ferroan serpentines or chlorites.

Halos around irregular-shaped troilites are observed in some magnesian chondrules or in phyllosilicate-rich clasts (Fig. 1–18). BSE images reveal that they are brighter than the surrounding low-Al magnesian phyllosilicates, because of their high FeO-content. However, these halos have textures similar to the surrounding magnesian phyllosilicates, and also contain Na_2O and K_2O (0.3–0.8%). They are more enriched in FeO than in the serpentine (Fig. 4). Thus, these halos are probably magnesian phyllosilicates contaminated by some Fe-bearing phases. These halos are common in Y-86720 (IKEDA *et al.*, 1992).

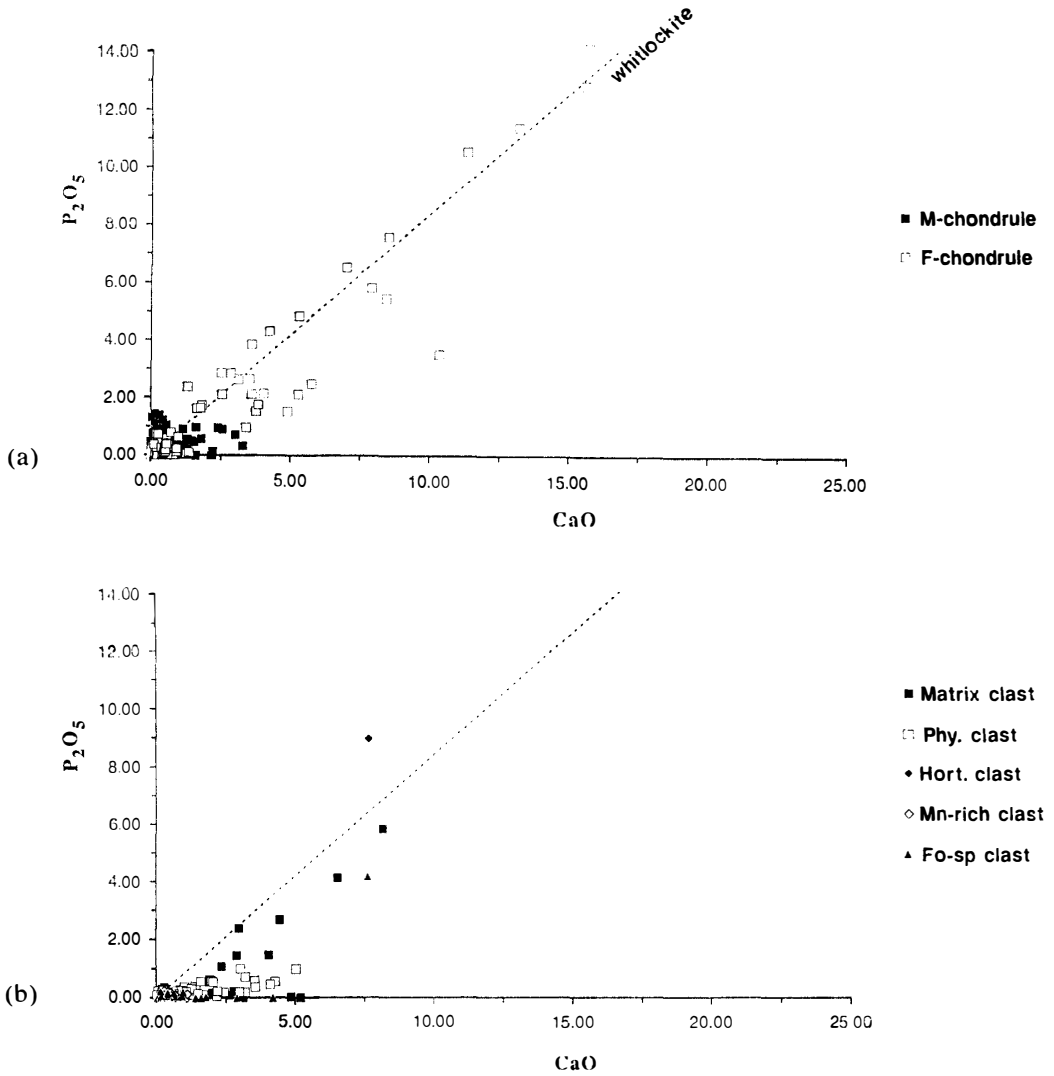

Fig. 6. CaO vs. P_2O_5 (wt%) plot of phyllosilicates (or mixture) in (a) magnesian (M) and ferroan (F) chondrules, (b) matrix-like (Matrix), phyllosilicate-rich (Phy), hortonolite-rich (Hort), Mn-rich olivine-bearing (Mn-rich), and forsterite-spinel

The most important difference in composition between the phyllosilicates in magnesian and ferroan chondrules is the abundance of CaO and P_2O_5 (Fig. 6). Phyllosilicates in magnesian chondrules are depleted in CaO and P_2O_5, whereas many phyllosilicates in ferroan chondrules are apparently enriched in these elements. The P_2O_5 is always positively related with the CaO in ferroan chondrules. The P_2O_5/CaO ratio for the phyllosilicates in the ferroan chondrules (about 0.85) suggests that a very fine-grained whitlockite component mixes with the phyllosilicates. The Cr_2O_3 content also differs between the phyllosilicates in the magnesian (0.1–2.0% and 1.0% on average) and the ferroan chondrules (0.1–0.8% and 0.5% on average). The high Cr_2O_3 content of the phyllosilicates in the magnesian chondrules may be the result of the contamination of tiny chromites in the phyllosilicates, whereas discrete coarse-grained chromite occurs in the ferroan chondrules.

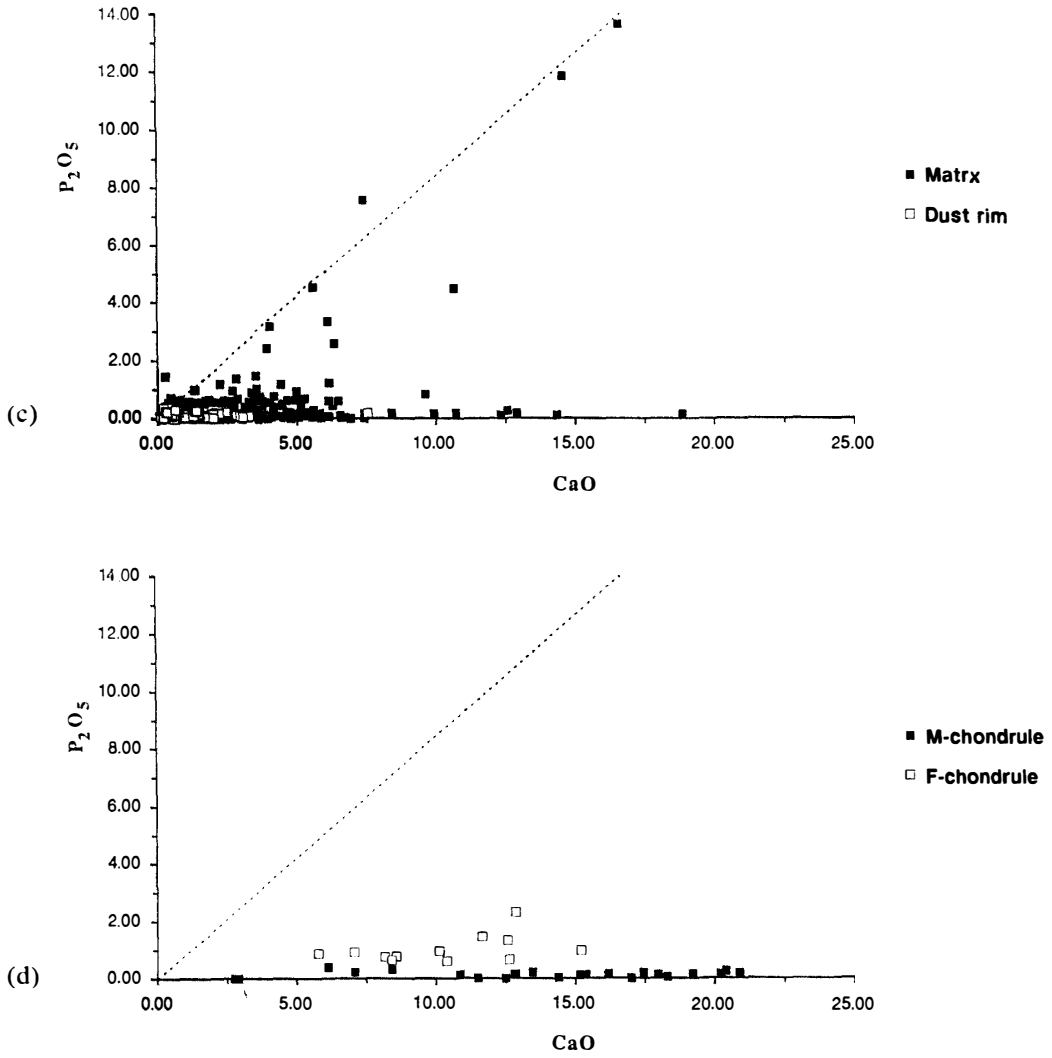

(Fo-sp) clasts, (c) the matrix and dust rims, and (d) glasses in magnesian (M) and ferroan (F) chondrules. Dotted line shows a mixing trend of whitlockite and phyllosilicate.

4.4.2. Phyllosilicate of Cr-rich ovoids in magnesian chondrules

Cr-rich ovoids are similar in composition to the low-Al phyllosilicates in chondrules, although they are more enriched in Cr_2O_3 (0.3–9.9%), as also noted by BISCHOFF and METZLER (1991). In addition, these phyllosilicates seem to have high contents of FeO (12.6–55.3%), NiO (0.0–9.8%), and P_2O_5 (0.0–6.8%). Therefore, they consist mainly of low-Al phyllosilicates which are contaminated by the very fine-grained opaque minerals such as chromite, taenite, schreibersite, and troilite. These ovoids seem to differ in composition and texture from the PCP in other CM chondrites that were described by TOMEOKA and BUSECK (1985). A Cr-rich ovoid has abundant troilites and a very fine-grained TiO_2-rich phase (10.0–13.8 wt% TiO_2), and may contain a Ti-oxide such as ilmenite.

4.4.3. Phyllosilicate in clasts and as an isolated mineral

Phyllosilicates occurring in silicate-rich clasts and as an isolated mineral are mostly of the low-Al magnesian type (Figs. 4 and 5), and similar to those in chondrules. Phyllosilicates in the hortonolite-rich, kamacite-rich, and some phyllosilicate-rich clasts are apparently ferroan. However, once again the ferroan nature may be due to contamination with Fe-bearing tiny minerals such as troilite, taenite, or magnetite. Forsterite-spinel clasts have high-Al magnesian phyllosilicates. Phyllosilicates in the Mn-rich olivine-bearing clasts are low in MnO (Table 3), and most of the MnO content resides in the olivine and chromite in these clasts. The compositions of phyllosilicates in matrix-like clasts are similar to those in the matrix and phyllosilicate-rich clasts. Some phyllosilicates in matrix-like clasts have CaO and P_2O_5 contents similar to those in ferroan chondrules, whereas other phyllosilicates in matrix-like clasts hardly contain P_2O_5 (Fig. 6).

4.4.4. Phyllosilicate in matrix and dust rims

Phyllosilicates in matrix and dust rims have similar compositions to one another (Figs. 4 and 5), and they are mostly low-Al magnesian type. Although some phyllosilicates in matrix and dust rims may be contaminated by opaque minerals such as magnetite and sulfide, phyllosilicates in matrix and dust rims are slightly richer in FeO than those in chondrules; average atomic Mg/Mg+Fe ratios of phyllosilicates in magnesian and ferroan chondrules, matrix, and dust rims are 0.70, 0.69, 0.63, and 0.64, respectively. The Cr_2O_3 content (0.2–0.9%) of the phyllosilicates in matrix and dust rims is similar to those in ferroan chondrules.

The Al_2O_3 and (Na_2O+K_2O) contents of the phyllosilicates in matrix and dust rims are different from those in the chondrules (Fig. 5); very low-alkali phyllosilicates occur in the matrix, but rarely in the chondrules, although alkali-bearing phyllosilicates in the matrix (along a line A-B) are similar in composition to those in chondrules and clasts. Thus, the matrix phyllosilicates seem to include Na-Al-talc (or mixed layer mineral) component in addition to serpentine component. Figure 4 also shows that phyllosilicates in the matrix include a Na-Al-talc component.

Matrix phyllosilicates in B-7904 show distinct compositional heterogeneities. Figure 7 shows that the matrix phyllosilicates in thin sections 92-1 and 92-2 are generally higher in Na+K than those in 92-3 and 94-2. Therefore, the matrix phyllosilicates in 92-1 and 92-2 are enriched in Na-Al-talc component, and those in 92-3 and 94-2 are enriched in serpentine component. Within one thin section,

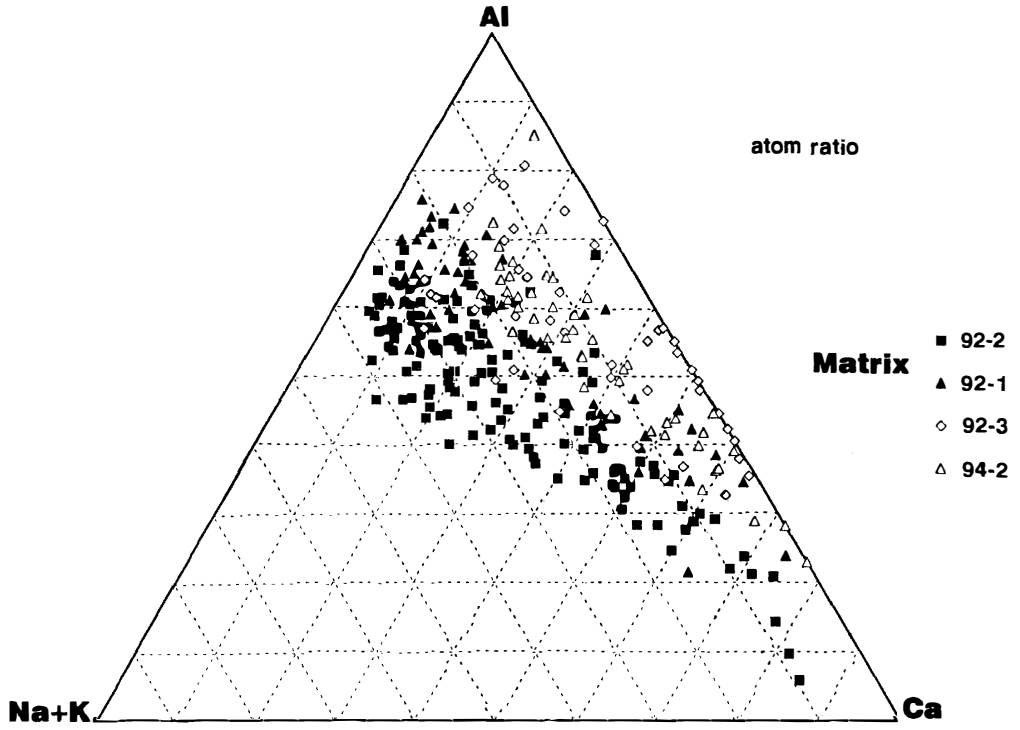

Fig. 7. Atomic Al-(Na+K)-Ca plot of matrix phyllosilicates including small amounts of phosphate and carbonate. Note that the compositions of matrix phyllosilicates are different among 4 thin sections of B-7904, and phyllosilicate compositions are heterogeneous within a thin section.

the compositional heterogeneity is relatively small, but the serpentine-enriched or Na-Al-talc-enriched phyllosilicates seem to be distributed within small areas of several tens of microns across.

Phyllosilicates in matrix and dust rims are apparently rich in CaO and often P_2O_5 (Fig. 6), and they may be mixed with whitlockite. Apparent low-P_2O_5 and high-CaO compositions are common in the matrix phyllosilicates, but never in chondrules. The apparent higher CaO phyllosilicates have a low total weight percent of major element oxides (for example, 18.9 wt% CaO and 81.7% total of a matrix phyllosilicate), suggesting that they may be mixed with Ca-carbonates. Although this study and TOMEOKA (1990) found only a few discrete carbonate grains in B-7904, many carbonate grains of submicron size may be abundantly mixed with the phyllosilicates in the B-7904 matrix. Ca-carbonate component is more common in the matrix than in the phosphate component.

4.5. Glass

Most of glass in B-7904 have similar compositions to chondrule glass in ordinary and C3 chondrites (Fig. 8). However, glass in magnesian and ferroan chondrules in B-7904 differ in composition from one another. Glasses in magnesian chondrules are more enriched in Al_2O_3 and CaO, and depleted in Na_2O, K_2O, and P_2O_5, than those in ferroan chondrules (on average, 19.9 wt% and 14.5 wt% of Al_2O_3, 13.7% and 9.9% CaO, 1.7% and 2.8% Na_2O, 0.0% and 0.3% K_2O, and 0.1% and 1.0%

P_2O_5, respectively). Glass in ferroan chondrules has a higher P_2O_5 than that in magnesian chondrules (Fig. 6d). One small glass inclusion in a magnesian chondrule is very enriched in SiO_2 (about 90%) with a small contents of CaO (2.9%) and

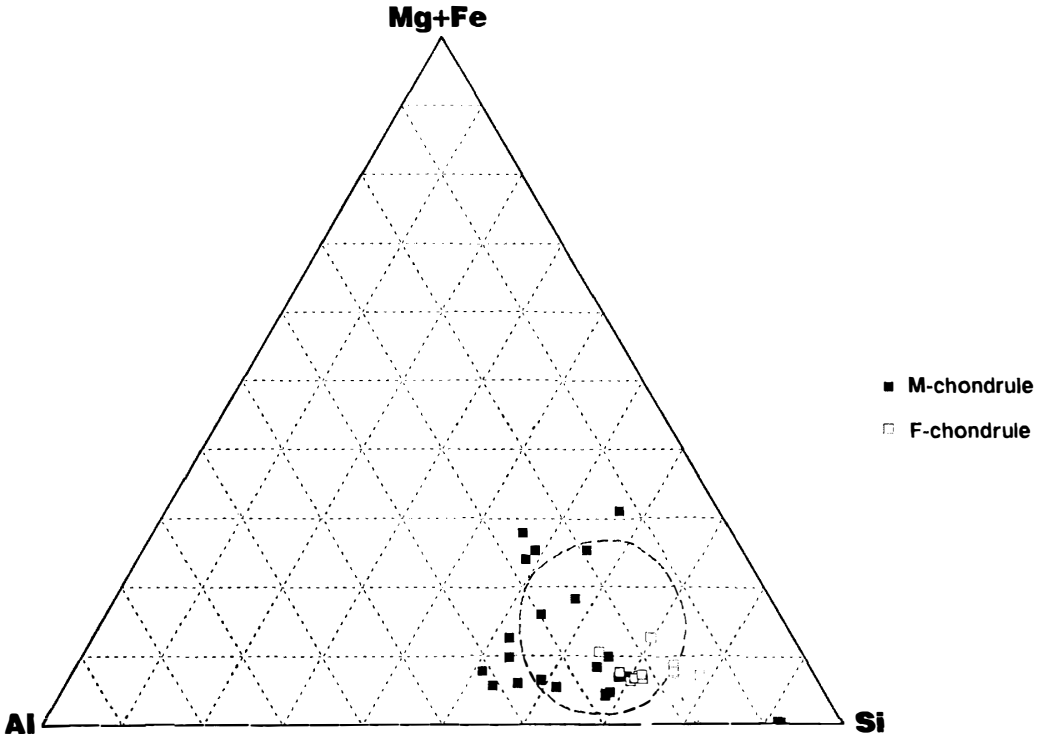

Fig. 8. Atomic (Mg+Fe)-Al-Si plot of glasses in magnesian (M) and ferroan (F) chondrules. The distribtion of glass in chondrules in unaltered chondrites, after IKEDA *(unpublished data), is shown by the broken line.*

Table 4. Representative compositions

Phase	Occurrence	SiO_2	TiO_2	Al_2O_3
Spinel	Magnesian chondrule	0.76	0.37	66.53
Spinel	Forsterite-rich clast	0.00	0.06	69.38
Spinel	Spinel-rich clast	0.00	0.53	71.28
Chromite	Ferroan chondrule	0.00	1.26	22.24
Chromite	Ferroan chondrule	0.00	0.81	5.43
Chromite	Matrix-like clast	0.16	1.41	6.16
Chromite	Mn-rich olivine-bearing clast	0.59	0.05	0.04
Eskolaite[1)]	Phyllosilicate-rich clast	1.64	0.03	0.13
Magnesiowüstite[2)]	Magnesian chondrule	0.00	0.09	0.11
Magnesiowüstite[2)]	Magnesian chondrule	0.00	0.00	0.18
Magnetite	Kamacite-rich clast	0.00	0.48	0.41
Magnetite[2)]	Kamacite-rich clast	0.00	1.47	1.44
Phosphate[2)]	Ferroan chondrule	0.27	0.03	0.00
Phosphate[2)]	Hortonolite-rich clast	0.90	0.00	0.01
Carbonate	Isolated mineral	0.48	0.00	0.10

[1)] Contaminated by surrounding phyllosilicate, because of the small grain size (see text).
[2)] The low totals are probably due to the small grain size (see text).

Al_2O_3 (6.4%) (Fig. 1–6), although we cannot exclude the possibility that this is a silica mineral contaminated by surrounding plagioclase.

4.6. Spinel and chromite

Spinel in forsterite-spinel clasts is a Mg-Al-spinel (Table 4 and Fig. 9) with small contents of Cr_2O_3 (0.1–0.5 wt%) and FeO (0.1–1.6%). A Mg-Al-spinel in forsterite phenocrysts in magnesian chondrules contains higher Cr_2O_3 (2.5%). All spinels in forsterite-spinel clasts and magnesian chondrules have low contents of TiO_2 (0.1–0.6%) and V_2O_3 (0.0–0.3%), and MnO and ZnO are below detection.

Chromites are divided into three types based on their chemistry, Al_2O_3-rich (3.3–23.2 wt% Al_2O_3), Al_2O_3-poor (0.3–0.6%), and MnO-rich (8.9–9.0% MnO and <0.05% Al_2O_3) types (Fig. 9). The Al_2O_3-rich chromites occur in ferroan chondrules, matrix-like clasts, and matrix. The chromites in ferroan chondrules are usually zoned; FeO and Al_2O_3 increase toward the rim, for example from 29.7% and 20.7% to 32.1% and 22.2%, respectively, although chromite in a ferroan chondrule has an Al_2O_3-poor (0.3%) rim. Fine-grained Al_2O_3-poor chromites, up to 3 microns, occur in Cr-rich ovoids in magnesian chondrules, phyllosilicate-rich clasts, and matrix. MnO-rich chromites occur only in a Mn-rich olivine-bearing clast. The Fe/Mg ratio and the V_2O_3 content (0.2–1.3%) of chromites in each type are similar. The Al_2O_3-rich chromites in ferroan chondrules have a lower ZnO content (0.0–0.3%) and a higher TiO_2 content (0.4–4.0%) than Al_2O_3-poor ones in magnesian chondrules (0.4–0.6% ZnO and <0.1% TiO_2).

4.7. Magnesiowüstite

Magnesiowüstite occurs within a troilite-taenite aggregate in the core of a magnesian chondrule (Fig. 1–9). Analyses of the oxygen, magnesium, and iron contents

of oxides, phosphate, and carbonate.

Cr_2O_3	V_2O_3	FeO	NiO	MnO	MgO	CaO	ZnO	Na_2O	P_2O_5	Total
2.50	0.08	0.42	0.00	0.00	27.13	0.59	0.00	0.00	0.00	98.38
0.49	0.06	0.14	0.00	0.00	28.00	0.00	0.05	0.00	0.00	98.19
0.09	0.20	0.41	0.00	0.06	27.49	0.06	0.00	0.00	0.00	100.13
37.11	0.90	32.06	0.10	0.37	4.49	0.00	0.18	0.01	0.06	98.78
58.87	0.63	27.75	0.09	0.39	5.43	0.00	0.14	0.04	0.03	99.62
53.53	0.83	33.85	0.21	0.19	1.78	0.13	0.10	0.00	0.33	98.68
68.09	0.14	15.30	0.10	9.03	5.73	0.04	0.21	0.08	0.07	99.50
91.03	0.49	2.93	0.13	0.19	1.05	0.10	0.06	0.15	0.22	98.17
0.22	0.00	69.04	0.27	0.11	26.15	0.07	0.12	0.00	0.06	96.24
0.28	0.02	69.63	0.21	0.06	23.66	0.15	0.00	0.00	0.05	94.25
0.03	0.00	88.91	0.10	0.00	1.44	0.00	0.00	0.00	0.00	91.38
0.14	0.00	82.15	0.19	0.22	2.26	0.05	0.00	0.02	0.10	88.04
0.05	0.00	1.32	0.00	0.00	3.55	45.70	0.00	1.03	41.01	92.95
0.00	0.02	3.79	0.07	0.06	3.18	41.72	0.00	1.81	38.54	90.15
0.00	0.00	0.39	0.00	0.00	2.91	45.41	0.00	0.59	0.10	49.98

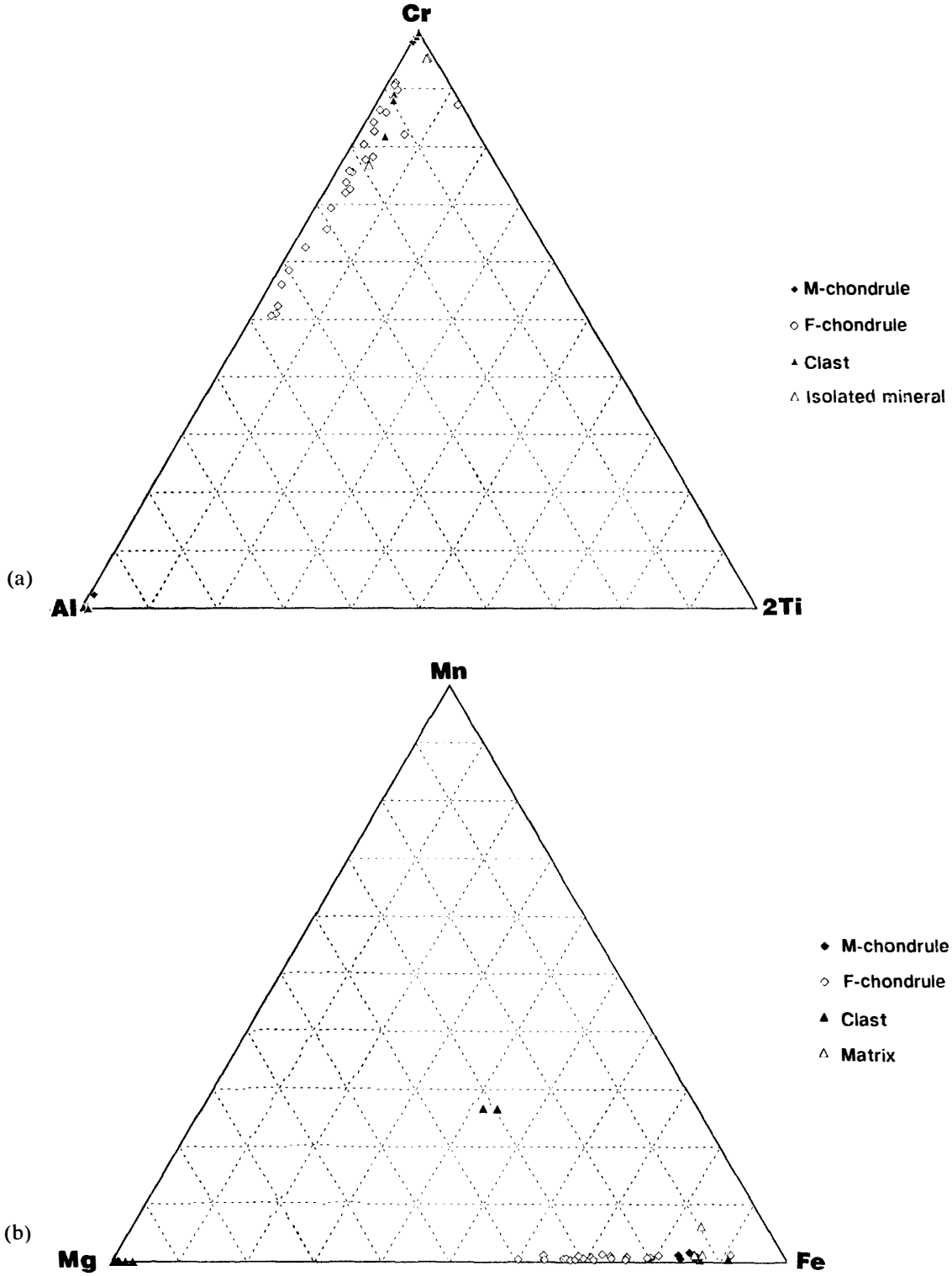

Fig. 9. Atomic plots of (a) Cr-Al-2Ti and (b) Mn-Mg-Fe for chromites and spinels in magnesian (M) and ferroan (F) chondrules, all silicate-rich clasts, and isolated minerals.

Table 5. Representative compositions of magnesiowüstite and magnetite in a magnesian chondrule.

Phase	O	Mg	Fe	Ni	Total	Formula
Magnetite	26.38	0.52	66.34	0.04	93.28	$(Fe_{2.88}Mg_{0.05})_{2.93}O_4$
Magnetite	25.91	0.52	67.02	0.04	93.49	$(Fe_{2.96}Mg_{0.05})_{3.01}O_4$
Magnesiowüstite	27.42	17.03	50.34	0.03	94.82	$(Fe_{0.53}Mg_{0.41})_{0.94}O_1$
Magnesiowüstite	27.30	15.96	52.02	0.08	95.36	$(Fe_{0.55}Mg_{0.38})_{0.93}O_1$

The low totals of magnetites and magnesiowüstites are probably due to their porous surfaces (Fig. 1-8) and the small grain size (Fig. 1-9), respectively.

give an average chemical formula of $(Fe_{0.54}Mg_{0.39})_{0.93}O_{1.00}$ (Table 5). They have <0.2 wt% of Al_2O_3 and CaO, <0.3% of Cr_2O_3 and NiO, <0.1% of TiO_2, MnO, and ZnO, and <0.05% of SiO_2 and V_2O_3. Magnesiowüstite has recently been reported from Vigarano (CV3) (CAILLET *et al.*, 1988) and Y-82162 chondrite (IKEDA, 1991). They are enriched in the periclase molecule (about $periclase_{70}wüstite_{30}$). However, magnesiowüstite obtained here has a lower periclase than wüstite molecule. IKEDA (1991) showed that magnesiowüstite in Y-82162 has a stoichiometric chemical composition with cation/oxygen atomic ratio of unity, whereas magnesiowüstite in B-7904 with the ratio of about 0.93/1.00 indicates non-stoichiometric. It is well known that Fe-poor wüstite has an ordered structure with non-stoichiometric composition, not a NaCl structure (LINDSLEY, 1976). Therefore, the magnesiowüstite obtained here may have a structure similar to the non-stoichiometric wüstite, being different in crystallographic structure from magnesiowüstites in Vigarano and Y-82162.

4.8. Magnetite

Magnetite occurs in kamacite-rich clasts and magnesian chondrules. The magnetite contains 0.0–2.9 wt% Cr_2O_3, 0.1–1.4% NiO, 1.4–7.7% MgO, and 0.0–1.4% Al_2O_3. Table 5 gives the analyses of the Mg, Fe, and O for the magnetites in association with kamacite and taenite in a magnesian chondrule, and an average chemical formula of $(Fe_{2.92}Mg_{0.05})_{2.97}O_4$.

4.9. Eskolaite

An irregular-shaped opaque mineral containing high Cr_2O_3 (81–91 wt%), and up to 3 microns across, occurs in B-7904. It may be eskolaite from the high content of Cr_2O_3, and it occurs only in the peripheral parts of Cr-rich ovoids in magnesian chondrules (Fig. 1-12) and a phyllosilicate-rich clast. We believe that the eskolaite was not introduced by contamination during sample preparation, because of (1) limited occurrences around Cr-rich ovoids and a phyllosilicate-rich clast, (2) the intimate association with phyllosilicate, and (3) impure Cr_2O_3. This is the first discovery of eskolaite in a meteorite. The EPMA analyses of the eskolaites apparently contain small amounts of SiO_2, Al_2O_3, and MgO (Table 4), but their ratios are similar to those of the surrounding phyllosilicate, and thus may be due to beam overlap during analysis. On the other hand, FeO seems to be present in the eskolaite (0.7–1.0%), even after taking the contamination into account. In addition, it contains V_2O_3 (0.3–1.4%) and ZnO (0.0–0.4%).

4.10. *Phosphate*

Phosphate grains occur in ferroan chondrules, some clasts, and in the matrix. The phosphate grains are too small for good analyses, but most of them may be whitlockite, based on their contents of MgO and Na_2O, and the Ca/P ratio (Table 4); they are Cl-free. On the other hand, all phosphates in a hortonolite-rich clast with kamacite and in a matrix-like clast, and a few phosphate grains in the matrix, contain 1–3% Cl; they are chlorapatite.

4.11. *Carbonate*

We found only a few irregularly-shaped grains of carbonate in the matrix (Fig. 1–27). They contain 36.2–45.4 wt% CaO, 0.8–6.3% FeO, and 2.8–2.9% MgO. Since contaminated SiO_2 is very low (<0.5%), and sulfur is not detected by qualitative analysis, the carbonates must have the small contents of FeO and MgO measured; MnO is below detection. They are Ca-carbonate.

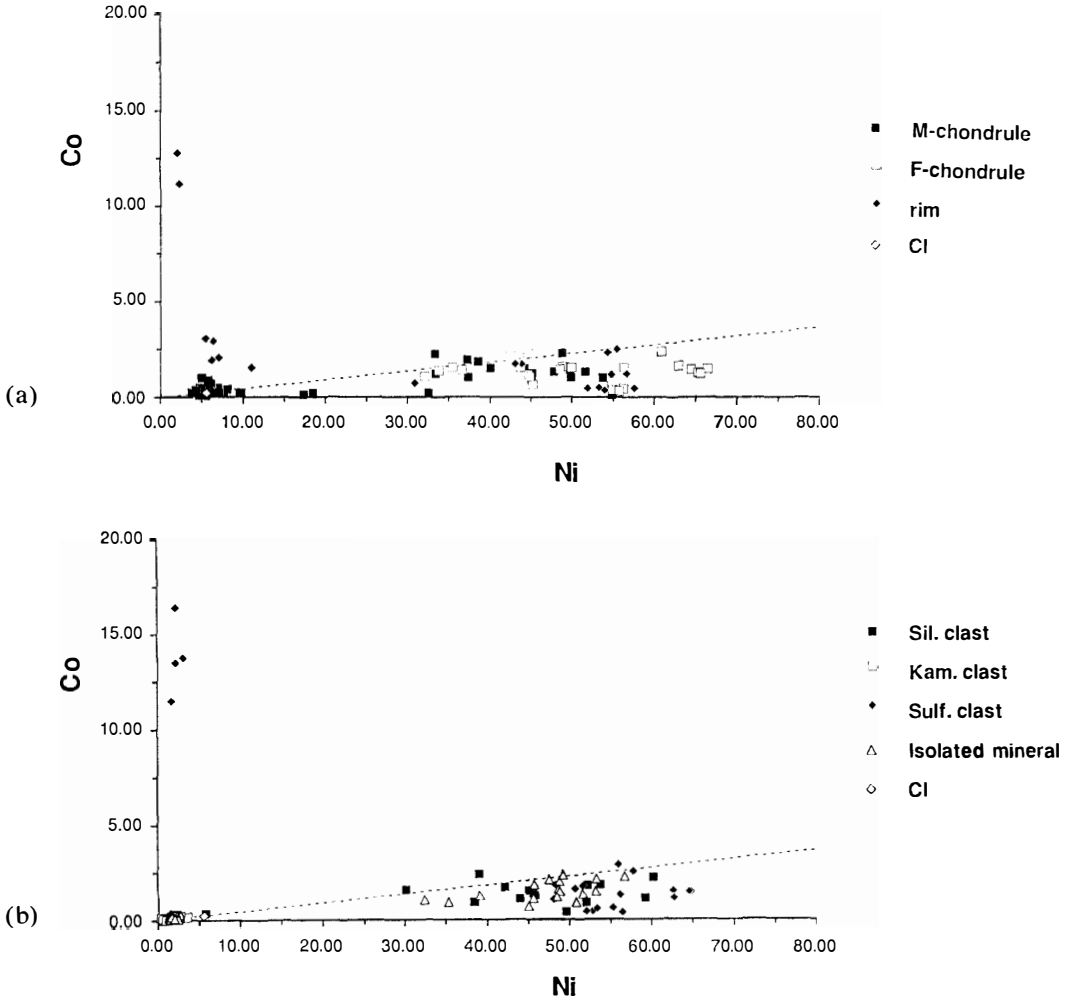

Fig. 10. Ni vs. Co (wt%) plot of Fe-Ni metals in (a) magnesian (M) and ferroan (F) chondrules, and sulfide-metal rim surrounding chondrules, and (b) silicate-rch (Sil), kamacite-rich (Kam), sulfide-rich (Sulf) clasts, and isolated minerals. CI line shows the Co/Ni ratio of average CI chondrite after ANDERS *and* GREVESSE *(1989).*

4.12. Fe-Ni metal

B-7904 has three kinds of Fe-Ni metal. These are kamacite, taenite (including tetrataenite and awaruite), and Co-rich metal. Table 6 gives the representative compositions. Kamacite is divided into two groups, a Ni-Co-rich group, and a Ni-Co-poor group (Fig. 10). Ni-Co-rich kamacite occurs in forsterite phenocrysts in magnesian chondrules and a phyllosilicate-rich clast, and the average weight % of Fe, Ni, and Co (93.7, 0.4, and 5.9) are similar to those of CI chondrite (94.3, 0.3, and 5.5 after ANDERS and GREVESSE, 1989), respectively, and contains 0.1–0.7 wt% P. Ni-Co-rich kamacites in B-7904 contain 0.1–0.7 wt% P. Some Ni-Co-rich kamacite has higher Co content (1.0–3.1%), and occurs with Co-poor (0.1–0.5%) taenite within troilite rims around a magnesian chondrule and within a kamacite-taenite-magnetite aggregate in a large magnesian chondrule (Fig. 1–8). Ni-Co-poor kamacite occurs in hortonolite-rich clasts, kamacite-rich clasts, and matrix. The Ni/Fe and Co/Fe ratios are lower than those in CI chondrites (Fig. 10). These kamacites are depleted in P (<0.1%).

Taenite has variable Ni and Co contents, and the Co content of taenite is usually higher than in the Ni-Co-rich and Ni-Co-poor kamacites (Fig. 10). Some taenite grains in chondrules, clasts, and the matrix are enriched in Ni, more than 50 wt.%. The Fe-Ni phase diagram obtained by REUTER *et al.* (1989) suggested that they may be awaruite, tetrataenite, or their mixture on a submicron-sized scale, although we could not identify these phases, due to their fine grain sizes. Therefore, we shall call all these Ni-rich metal taenite for convenience.

Co-rich metal is rich in Co (11.5–16.3%) and poor in Ni (1.7–3.2%). It was also reported in Ngawi LL3 chondrite (AFIATTALAB and WASSON, 1980), and from some LL3–6 chondrites (RUBIN, 1990). AFIATTALAB and WASSON found two kinds of Co-rich phases, phase X (12% Co and 3% Ni) and phase Y (37%

Table 6. Representative compositions of metal and sulfides.

Phase	Occurrence	P	Si	S	Cr	Fe	Co	Ni	Total
Kamacite	Magnesian chondrule	0.32	0.03	0.00	0.19	92.69	0.47	6.15	99.85
Kamacite	Magnesian chondrule	0.51	0.03	0.02	0.06	93.66	0.56	5.30	100.13
Kamacite	Hortonolite-rich clast	0.04	0.06	0.06	0.00	96.78	0.02	1.09	98.05
Kamacite	Kamacite-rich clast	0.00	0.04	0.00	0.00	98.42	0.00	0.63	99.09
Kamacite	Isolated mineral	0.02	0.01	0.00	0.00	97.46	0.11	1.44	99.03
Taenite[1)]	Magnesian chondrule	0.02	0.00	0.20	0.00	43.40	0.11	54.86	98.60
Taenite[2)]	Ferroan chondrule	0.00	0.03	0.31	0.07	34.74	2.39	60.85	98.39
Taenite[3)]	Sulfide-rich clast	0.00	0.06	0.00	0.07	31.67	1.48	64.58	97.87
Co-rich metal	Sulfide-rich clast	0.00	0.04	0.16	0.10	81.73	16.34	2.19	100.56
Schreibersite	Magnesian chondrule	15.52	0.00	0.18	0.00	74.83	0.25	9.70	100.48
Troilite	Magnesian chondrule	0.00	0.00	36.98	0.07	63.49	0.04	0.11	100.69
Troilite	Ferroan chondrule	0.00	0.01	35.86	0.00	62.12	0.07	0.23	98.29
Pentlandite	Ferroan chondrule	0.00	0.00	32.84	0.00	45.42	0.57	19.87	98.71
Pentlandite	Ferroan chondrule	0.00	0.10	33.23	0.07	46.20	0.48	18.80	98.89

[1)] or tetrataenite (see text)
[2)] or mixture of tetrataenite and awaruite
[3)] or awaruite

Co and 8.5% Ni). The former probably has kamacite structure, and the latter is an ordered Fe-Co metal. Although phase Y was not found in B-7904, the Co-rich metal obtained here may correspond to phase X found by AFIATTALAB and WASSON (1980).

4.13. Schreibersite

Schreibersite occurs rarely in forsterite phenocrysts and Cr-rich ovoids of magnesian chondrules, and in Mn-rich olivine-bearing clasts. This is the first discovery of schreibersite in CM chondrites. Schreibersite occurring with taenite in Cr-rich ovoids and Mn-rich olivine-bearing clasts is more enriched in Ni (33–44 wt%) than the (9.5–17.3%) in association with kamacite in forsterite phenocrysts of magnesian chondrules.

4.14. Sulfide

Troilite occurs in all of the components of B-7904, and has an average chemical formula of $Fe_{1.01}S_1$. Pentlandite occurs in chondrules, sulfide-rich clasts, some silicate-rich clasts, and sulfide rims around chondrules, and as an isolated mineral. The composition of pentlandite does not depend on their occurrences such as chondrules, clasts, and isolated mineral, and they contain 13.3–20.4 wt% Ni and 0.1–0.9% Co. Average chemical formula of the pentlandite is $(Fe_{6.53}Ni_{2.44}Co_{0.07})_{9.04}S_8$, which resembles that obtained by ZOLENSKY *et al.* (1989).

5. Discussion

Phyllosilicate occurs abundantly in most of the components in B-7904, suggesting that B-7904 has experienced hydrous alteration, as did other CM chondrites. However, some components and minerals in B-7904 escaped extensive alteration. For example, well-shaped chondrules occur abundantly, and preserve their primary texture. Glass in olivine phenocrysts remains unaltered. Thus, this meteorite has partly preserved its primary features, and we will discuss the features of the components in addition to the hydrous alteration, and the genetic relationships among the components in B-7904. Figure 11 summarizes the genetic relationships of these components.

5.1. Formation of magnesian chondrules

Magnesian chondrules have kamacite inclusions in forsterite phenocrysts, whereas the groundmass has taenite and troilite, suggesting that the kamacite inclusions in phenocrysts have escaped from sulfurization to form troilite in the groundmasses.

The Ni and Co contents of kamacite inclusions in magnesian chondrules are similar to those of CI chondrites (Fig. 10a), suggesting that this kamacite formed primarily from a gas of the solar composition. Phosphorous is contained only in kamacite and schreibersite in magnesian chondrules, and the presence of metallic P supports the idea that magnesian chondrules formed under reducing conditions. Forsterite in magnesian chondrules has MnO/FeO ratios higher than that of CI chondrites (Fig. 2). KLÖCK *et al.* (1989) found such olivines in some unequilibrated

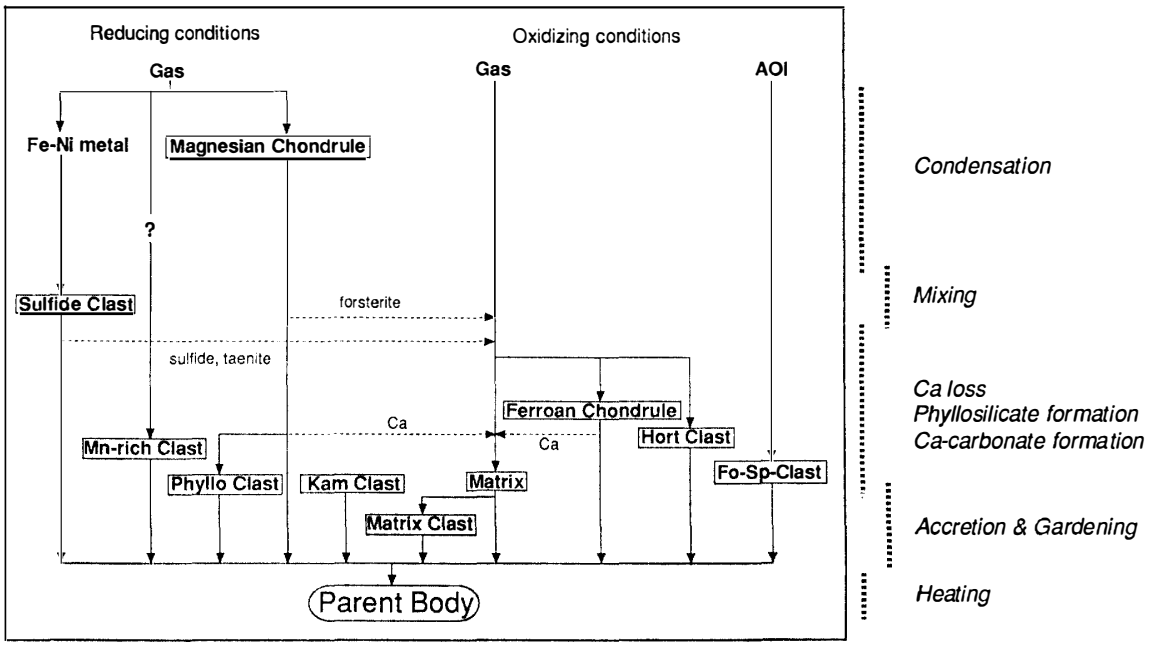

Fig. 11. Schematic diagram showing genetic relationships among two kinds of chondrules, seven kinds of clasts, and matrix in B-7904. Phyll Clast: phyllosilicate-rich clast, Mn-rich Clast: Mn-rich olivine-bearing clast, Matrix Clast: matrix-like clast, Hort Clast: hortonolite-rich clast, Kam Clast: kamacite-rich clast, Fo-Sp-Clast: forsterite-spinel clast. At the right, major processes for the formation of B-7904 are shown for reference (see text).

chondrites and interplanetary dust, and concluded that they condensed from a gas of the canonical solar composition under reducing conditions. This supports our idea that the precursors of magnesian chondrules in B-7904 were produced as condensates in the solar nebula under reducing conditions.

One large magnesian chondrule includes an aggregate of magnetite, kamacite, and taenite. Textural observation (Fig. 1–8) indicates that kamacite and taenite may have been later oxidized to form magnetite. The geothermometer obtained by AFIATTALAB and WASSON (1980) using Co partitioning between the coexisting kamacite (2.9 wt% Co) and taenite (0.4%) gives the equilibration temperature of 660±20 K, which corresponds to the temperature during the oxidation to form magnetite. In addition, this chondrule includes an aggregate of troilite-taenite-magnesiowüstite near the aggregate of magnetite-kamacite-taenite. On the assumption that the magnesiowüstite, magnetite, and kamacite were equilibrated within this chondrule, the equilibration temperature and oxygen partial pressure were calculated by the following equations;

$$\underset{\text{kam}}{Fe} + 1/2\underset{}{O_2} = \underset{\text{wüs}}{FeO}, \qquad (1)$$

and

$$\underset{\text{kam}}{3Fe} + 2\underset{}{O_2} = \underset{\text{mag}}{Fe_3O_4}, \qquad (2)$$

where kam, wüs, and mag are kamacite, wüstite, and magnetite, respectively. The

thermodynamic data (ROBIE *et al.*, 1979) were used with an assumption that the magnesiowüstite $(Fe_{0.6}Mg_{0.4})O$ is an ideal solution with activity of 0.6 for the FeO component. The calculated temperature and oxygen partial pressure are 656 K and 10^{-36} bars, respectively. This temperature is well consistent with the equilibration temperature (660 K) for the kamacite-taenite pairs mentioned above. The oxygen partial pressure for reactions (1) and (2) is much higher than that (*ca.* 10^{-43} bars) of the solar gas with a 10^{-4} bars total pressure at 600 K (GROSSMAN, 1972). Thus, the oxidation reaction took place under a much more oxidizing condition than the solar gas. Magnesian chondrules, which had primarily originated under a reducing condition, have later mixed with ferroan chondrules and matrix, and experienced oxidation reactions during the hydration.

Glass inclusions in forsterite phenocrysts of magnesian chondrules always contain CaO. The glass in phenocrysts has preserved the primary groundmass compositions, because they have similar compositions to groundmasses in chondrules of unaltered chondrites (Fig. 8). On the other hand, phyllosilicates in chondrules, which were produced from the groundmass glass, are nearly CaO-free. Therefore, CaO may have been lost from chondrules during hydrous alteration.

Cr-rich ovoids in magnesian chondrules in B-7904 have higher SiO_2 and MgO contents than PCP in other CM chondrites, and show a textures different from PCP (TOMEOKA and BUSECK, 1985). The occurrence and mineralogy of Cr-rich ovoids suggest that they may have been produced from metal-sulfide spherules in original chondrules by hydration, because they have similar outlines to metal-sulfide spherules in chondrules in unaltered chondrites.

Halos are found around troilites in phyllosilicates of a few chondrules and clasts (Fig. 1–18), and they may have formed by contamination of an Fe-bearing phase, as noted in Section 4.4.1. Such halos occur abundantly in Y-86720, where the formation of the halos took place after the final aggregation of the Y-86720 chondrite (IKEDA *et al.*, 1992). However, the halos in B-7904 are not observed in most of chondrules and clasts including troilite grains, and in the matrix, and may have formed locally in some chondrules and clasts before final agglomeration of B-7904.

5.2. *Formation of ferroan chondrules*

Olivine in ferroan chondrules has MnO/FeO ratios similar to that of CI chondrites (Fig. 2a), suggesting that the precursors were similar in Mn and Fe contents to those of CI chondrites and the crystallization took place under conditions such that most of the Fe existed as FeO. Olivine phenocrysts in ferroan chondrules include taenite and troilite inclusions, and no kamacite, contrasting with forsterite phenocrysts including kamacite inclusions in magnesian chondrules. These suggest that ferroan chondrules had crystallized under a more oxidizing condition than magnesian chondrules, probably between the Fe-FeO buffer and Ni-NiO buffer. Probably the precursors of ferroan chondrules formed at lower temperatures, and under more oxidizing conditions than those of magnesian chondrules in the nebula. The presence of Ca-phosphate in ferroan chondrules, instead of schreibersite in magnesian chondrules, is consistent with oxidizing conditions. In addition, fine-grained phosphate and glass inclusions containing P_2O_5 are included in olivine

phenocryst of ferroan chondrules, suggesting that the phosphate component was originally incorporated in the precursor materials of ferroan chondrules.

Olivine in ferroan chondrules often has a magnesian core (Fo_{95-99}). These forsteritic cores have a low abundance, and do not always occur in the core of large ferroan olivine phenocrysts. It is plausible that they were originally fragments of forsterite phenocrysts which were produced by disaggregation from magnesian chondrules.

Ferroan chondrules were also altered to form phyllosilicates in the groundmass. Although ferroan chondrules have glass enriched in CaO (9.9% on the average), phyllosilicates produced by hydrous alteration in ferroan chondrules are depleted in CaO. Therefore, most of the CaO were lost from ferroan chondrules as well as magnesian chondrules. However, original phosphates in ferroan chondrules did not decompose during hydrous alteration, and survived during the CaO-free phyllosilicate formation.

A few ferroan chondrules have wollastonite in thin peripheral parts of some olivine phenocrysts (Fig. 1–30), and the olivine in contact with wollastonite is more magnesian (Fo_{55}) than other area of the olivine (Fo_{47}) suggesting that the wollastonite formed under reducing conditions. The CaO content of the wollastonite may have been supplied by the decomposition of the phosphate in the groundmass, because phosphate is a unique CaO-bearing phase adjacent to such olivine phenocrysts including wollastonite. Thus, this reduction may have taken place locally between phenocryst rims and groundmass phosphate, after the consolidation of these chondrules.

5.3. Formation of silicate-rich type clasts

Phyllosilicate-rich clasts have several mineralogical features similar to magnesian chondrules, such as the presence of forsterite, schreibersite, eskolaite, Al_2O_3-depleted chromite, and kamacite inclusions in forsterite. Therefore, they may be altered fragments of magnesian chondrules.

Mn-rich olivine-bearing clasts may have formed under reducing conditions similar to those of magnesian chondrules, because they also have schreibersite and forsteritic olivine. The Mn-rich olivines have MnO/FeO ratios similar to those of forsteritic olivines in magnesian chondrules (Fig. 2), suggesting that Mn-rich olivine-bearing clasts were cogenetic with magnesian chondrules. Therefore, we suppose that fractional condensation of Mn-poor forsterite in the solar nebula may have produced a MnO-rich condensate, which was the precursor of the Mn-rich olivine-bearing clasts.

On the other hand, hortonolite-rich clasts have a mineralogy similar to ferroan chondrules. These clasts have ferroan olivine, phosphate, troilite, and taenite, although these clasts are almost phyllosilicate-free. The similarity in mineralogy between this clast type and ferroan chondrules suggests that they had an intimate genetic relationship. Thus, it is possible that hortonolite-rich clasts formed from the same precursor materials as ferroan chondrules, or by some secondary modification from ferroan chondrules such as shock heating before incorporation into the parent body.

Matrix-like clasts resemble the matrix in mineralogy and texture, and they may have formed from the matrix material during regolith gardening, and were later agglomerated into the regolith.

Forsterite-spinel clasts have texture and mineralogy similar to amoeboid olivine inclusions (AOI's) in other carbonaceous chondrites, suggesting that they had primarily originated as AOI's in the solar nebula. These clasts often have a small amount of phyllosilicates in the interstices between forsterite and spinel, and also have experienced hydrous alteration.

As discussed before, the components of B-7904 probably originated in various reservoirs with contrasting fO_2 in the solar nebula. Magnesian chondrules, phyllosilicate-rich clasts, and Mn-rich olivine-bearing clasts have formed under reducing conditions. On the other hand, ferroan chondrules and hortonolite-rich clasts formed under much more oxidizing conditions than magnesian chondrules and others. All these components later mixed with one another.

5.4. Formation of opaque mineral-rich clast types

Sulfide-rich clasts consist of troilite, pentlandite, and taenite, often with Co-rich metal. Sulfide-metal rims surrounding chondrules have the same mineralogy as the sulfide-rich clasts, indicating that the sulfide-rich clasts and the rims have the same origin. TOMEOKA (1990) suggested that some troilite grains have been transformed from poorly-characterized phase (PCP) by heating. However, the sulfide-rich clasts and the rims do not have any other phases, such as silicates, phosphates, and oxides. This observation indicates that they may have not originated from PCP by heating, because PCP in ordinary CM chondrites always contain SiO_2, Al_2O_3, and MgO (TOMEOKA and BUSECK, 1985), and do not occur as rims of chondrules.

Alternatively, it is possible that the sulfide-rich clasts were produced from kamacite aggregates by sulfurization, because their compositions are mainly Fe with minor Ni and Co, except for S. If so, Co-rich metal and taenite pairs, which are found only in the sulfide-rich clasts and sulfide-metal rims, must have formed during the sulfurization; By sulfurization, primary kamacite, which had been formed as a condensate from a nebular gas under reducing conditions, may have been changed mainly into troilite (or hexagonal pyrrhotite of 1C structure above 140°C after YUND and HALL, 1968), and the Ni content went into newly formed taenite and pentlandite, resulting in that most of the Co were partitioned into Co-rich metal, and minor Co into taenite. The application of the geothermometer by AFIATTALAB and WASSON (1980) indicates that Co-rich metal (13.7–14.1% Co) and taenite (1.3–1.8% Co) pairs in the B-7904 sulfide-rich clasts formed at about 660–610 K, which is consistent with that of troilite condensation in the solar gas (GROSSMAN and LARIMER, 1974).

Kamacite-rich clasts consist mainly of Ni-Co-depleted kamacite with small amounts of troilite, magnetite, and phyllosilicates. The Ni-Co-depleted kamacite might have formed secondarily from some FeO-bearing sulfide, carbonate, oxide, or hydroxide. TOMEOKA *et al.* (1989) and IKEDA *et al.* (1992) concluded that Ni-Co-poor kamacites in Y-86720, which are similar in composition to those in B-7904, formed from ferrihydrites by heating.

5.5. The matrix and isolated minerals

The matrix phyllosilicates include Na-Al-talc (or mixed layer mineral) component in addition to serpentine component, as already mentioned in Section 4.4.4. The Na-Al-talc component has not yet been reported from the matrix phyllosilicate in B-7904. Phyllosilicates in the matrix of B-7904 have been considered to be serpentine (*e.g.*, KOJIMA *et al.*, 1984). They analyzed the matrix using a defocused beam (10–40 microns in diameter) of EPMA. Their analyses of the matrix were probably contaminated by isolated opaque minerals abundantly occurring in the matrix, and the B-7904 matrix phyllosilicates obtained by them seem to be too Fe-rich.

One of the most important mineralogical and petrological characteristics of B-7904 is the leaching of CaO from chondrules and clasts (Fig. 6). As already discussed in Sections 5.2 and 5.3, hydration to form the phyllosilicates had also lost most of the original CaO contents from magnesian and ferroan chondrules. The expelled CaO may be incorporated mainly as carbonates in the matrix. IKEDA *et al.* (1991) suggested that phyllosilicates in B-7904 chondrules and clasts were produced by hydrous reactions with a solar nebular gas. Thus, the loss of the CaO from magnesian chondrules and other components probably occurred in the nebula before the accretion to the parent body. This is consistent with the idea that CaO-loss from glass in chondrules in some C3 chondrites took place in the nebula (IKEDA and KIMURA, 1985).

The MnO/FeO weight ratios of the matrix (0.011 on the average) are similar to those of ferroan olivines (0.011 on the average) in ferroan chondrules, suggesting that the matrix has an intimate genetical relationship to the ferroan chondrules or their precursors. The phosphate component in the matrix may have been derived from ferroan chondrules by disaggregation, because Ca-phosphate abundantly occurs in ferroan chondrules. Alternative idea is that the phosphate component had been primarily included in the precursor materials of the matrix as well as ferroan chondrules.

There are abundant isolated minerals of silicate, oxide, sulfide, and Fe-Ni metal in the matrix. Isolated olivines in the matrix have the same compositional range as those in chondrules and clasts (Fig. 2). As mentioned before, isolated chromite, Fe-Ni metal, and sulfide grains also have similar compositions to those in chondrules and clasts, respectively. Therefore, most of isolated minerals were derived from chondrules and clasts by disaggregation.

5.6. Thermal metamorphism of B-7904

Some evidence for the thermal metamorphism of B-7904 has been presented by several authors. AKAI (1990) suggested that from comparison with heating experiments on the dehydration of the Murchison serpentine under vacuum conditions, B-7904 was heated to at least 750°C. On the other hand, ZOLENSKY *et al.* (1991) concluded that the heating temperature of B-7904 was below 600°C, based on their heating experiments on the Murchison meteorite under 10^{-4} bars H_2. PAUL and LIPSCHUTZ (1989) suggested that B-7904 was heated at 600–700°C, based on the pattern of labile trace elements. TOMEOKA (1990) suggested that some troilite

grains were formed from pre-existing PCP as a result of the metamorphism.

On the other hand, there is some evidence against thermal metamorphism. JOHNSON and PRINZ (1991) showed that chromite-olivine pairs in B-7904 chondrules keep their magmatic temperatures of about 1400°C, and that the chondrules experienced little reheating, similar to those in type 3.0–3.1 chondrites. In addition, we have found that diopside coexists with enstatite in a magnesian chondrule (Fig. 1–3 and Table 3a), and the two pyroxene geothermometer of LINDSLEY and ANDERSEN (1983) gives an equilibration temperature higher than 1300°C for the pyroxene pair. These magmatic temperatures are inconsistent with the high-temperature metamorphism of B-7904 suggested by AKAI (1990) and others.

Some forsterite fragments in the matrix do not have any ferroan rims around them, indicating that no reaction and diffusion may have occurred after the final agglomeration of B-7904 in the parent body. In addition, there are many chondrules and clasts showing unequilibrated mineral assemblages such as schreibersite-phosphate, forsterite-fayalite, and kamacite-phyllosilicate in B-7904. Glass in B-7904 does not show any devitrification textures. These observations also argue against thermal metamorphism of long duration.

However, phyllosilicates in all of the components of B-7904 were evidently decomposed to form submicroscopic secondary olivine (KOJIMA *et al.*, 1984; AKAI, 1988; TOMEOKA, 1990). Therefore, it is probable that B-7904 experienced heating in the parent body only for a short period of time. BISCHOFF and METZLER (1991) also suggested a short heating duration based on the wide variation in primary olivine compositions. Thus, the constituent minerals in B-7904 have not been homogenized by the heating in the parent body. A shock-event is the most plausible mechanism for this heating of short duration. LANGE *et al.* (1985) showed that antigorite shocked up to 45 GPa lacks petrographically observable shock indicators, although a significant amount of H_2O was driven out of the antigorite. This is consistent with the observation of B-7904 phyllosilicates that preserve the texture and chemistry of original phyllosilicates in the scale larger than micron size, except for H_2O. B-7904 may have experienced shock-events with pressures lower than 45 GPa.

6. Conclusions

(1) In comparison with Y-82161, -86720, and other CM chondrites, B-7904 has abundant primary components which experienced little hydrous alteration. Chondrules and AOI's preserve their primary textures. Although phyllosilicate which was produced by hydrous alteration is predominant, the components of B-7904 have various unaltered phases; phenocrystic olivine, euhedral chromite, glass, Ca-poor and -rich pyroxenes, plagioclase, Co-Ni-rich kamacite, Co-rich metal, schreibersite, and so on.

(2) B-7904 consists of various kinds of the components. Chondrules in B-7904 are divided into magnesian and ferroan types. Magnesian chondrules formed primarily under reducing conditions, whereas ferroan chondrules formed under oxidizing conditions. Phyllosilicate-rich and Mn-rich olivine-bearing clasts also

originated under conditions similar to those of magnesian chondrules. Hortonolite-rich clast and the matrix formed under oxidizing conditions. Therefore, B-7904 is a mixture of various components, which formed under contrasting fO_2.

(3) Magnesian chondrules and phyllosilicate-rich clasts have lost their original CaO completely during hydrous alteration to form phyllosilicate. Ferroan chondrules lost most of their original CaO, although the primary phosphate component was stable during alteration. All of the CaO lost from the components was later concentrated into the matrix to form the carbonates.

(4) In addition to hydrous alteration to form phyllosilicate, the oxidation reaction to form magnetite and magnesiowüstite from kamacite took place in a magnesian chondrule at about 660 K and 10^{-36} bars oxygen partial pressure, which is much higher than an oxygen partial pressure (*ca.* 10^{-43} bars) of the solar gas with a total pressure of 10^{-4} bars at 600 K. This suggests that magnesian chondrules were oxidized probably after mixing with ferroan chondrules and matrix prior to accretion to the parent body.

(5) B-7904 was reheated for a short duration, probably by shock effect. Although the phyllosilicates were dehydrated and secondary tiny olivine formed from the decomposed phyllosilicates, most of the constituent minerals were not largely affected by this heating event.

Acknowledgments

We thank Drs. K. YANAI and H. KOJIMA for sample allocations, and an anonymous referee for helpful reviews. This study has been supported by a Grant-in-Aid for Scientific Research from the Ministry of Education, Science and Culture (to Y. IKEDA).

References

AFIATTALAB, F. and WASSON, J. T. (1980): Composition of the metal phases in ordinary chondrites: Implications regarding classification and metamorphism. Geochim. Cosmochim. Acta, **44**, 431–446.

AKAI, J. (1988): Incompletely transformed serpentine-type phyllosilicates in the matrix of Antarctic CM chondrites. Geochim. Cosmochim. Acta, **52**, 1593–1599.

AKAI, J. (1990): Thermal metamorphism in four Antarctic carbonaceous chondrites and its temperature scale estimated by T-T-T diagram. Papers Presented to the 15th Symposium on Antarctic Meteorites, May 30–June 1, 1990. Tokyo, Natl Inst. Polar Res., 86–87.

ANDERS, E. and GREVESSE, N. (1989): Abundances of the elements: Meteoritic and solar. Geochim. Cosmochim. Acta, **53**, 197–214.

BISCHOFF, A. and METZLER, K. (1991): Mineralogy and petrography of the anomalous carbonaceous chondrites Yamato-86720, Yamato-82162, and Belgica-7904. Proc. NIPR Symp. Antarct. Meteorites, **4**, 226–246.

CAILLET, C., MACPHERSON, J. I., VELDE, D. and EL GORESY, A. (1988): Fremdlinge in Vigarano CAI 477B: Assemblages, compositions, and possible formational history. Lunar Planetary Science XIX. Houston, Lunar Planet. Inst., 156–157.

GROSSMAN, L. (1972): Condensation in the primitive solar nebula. Geochim. Cosmochim. Acta, **36**, 597–619.

GROSSMAN, L. and LARIMER, J. W. (1974): Early chemical history of the solar system. Rev. Geophys. Space Phys., **12**, 71–101.

HARAMURA, H., KUSHIRO, I. and YANAI, K. (1983): Chemical compositions of Antarctic meteorites I. Mem. Natl Inst. Polar Res., Spec. Issue, **30**, 109–121.

IKEDA, Y. (1991): Petrology and mineralogy of the Yamato-82162 chondrite (CI). Proc. NIPR Symp. Antarct. Meteorites, **4**, 187–225.

IKEDA, Y. and KIMURA, M. (1985): Na-Ca zoning of chondrules in Allende and ALHA-77003 carbonaceous chondrites. Meteoritics, **20**, 670–671.

IKEDA, Y., MAYEDA, T., CLAYTON, R. N. and PRINZ, M. (1991): Petrography and oxygen isotopic compositions of chondrules, clasts, and the matrix separated from Belgica-7904 and Yamato-86720 carbonaceous chondrites. Papers Presented to the 16th Symposium on Antarctic Meteorites, June 5–7, 1991. Tokyo, Natl Inst. Polar Res., 82–84.

IKEDA, Y., NOGUCHI, T. and KIMURA, M. (1992): Petrology and mineralogy of the Yamato-86720 carbonaceous chondrite. Proc. NIPR Symp. Antarct. Meteorites, **5**, 136–154.

JOHNSON, C. A. and PRINZ, M. (1991): Chromite and olivine in type II chondrules in carbonaceous and ordinary chondrites: Implications for thermal histories and group differences. Geochim. Cosmochim. Acta, **55**, 893–904.

KALLEMEYN, G. W. (1988): Compositional study of carbonaceous chondrites with CI-CM affinities. Papers Presented to the 13th Symposium on Antarctic Meteorites, June 7–9, 1988. Tokyo, Natl Inst. Polar Res.. 132–134.

KLÖCK, W., THOMAS, K. L., MCKAY, D. S. and PALME, H. (1989): Unusual olivine and pyroxene composition in interplanetary dust and unequilibrated ordinary chondrites. Nature, **339**, 126–128.

KOJIMA, H., IKEDA, Y. and YANAI, K. (1984): The alteration of chondrules and matrices in new Antarctic carbonaceous chondrites. Mem. Natl Inst. Polar Res., Spec. Issue, **35**, 184–199.

LANGE, M. A., LAMBERT, P. and AHRENS, T. J. (1985): Shock effects on hydrous minerals and implications for carbonaceous meteorites. Geochim. Cosmochim. Acta, **49**, 1715–1726.

LINDSLEY, D. H. (1976): The crystal chemistry and structure of oxide minerals as exemplified by the Fe-Ti oxides. Oxide Minerals, ed. by D. RUMBLE III. Blacksburg, Mineralogical Society of America, L1–L60.

LINDSLEY, D. H. and ANDERSEN, D. J. (1983): A two-pyroxene thermometer. Proc. Lunar Planet. Sci. Conf., 13th, A887–A906 (J. Geophys. Res., **38**, Suppl.).

MATSUNAMI, S., NISHIMURA, H. and TAKESHI, H. (1989): Compositional heterogeneity of alteration products in B-7904 chondrite. Papers Presented to the 14th Symposium on Antarctic Meteorites, June 6–8, 1989. Tokyo, Natl Inst. Polar Res., 21.

MAYEDA, T. K., CLAYTON, R. N. and YANAI, K. (1987): Oxygen isotopic compositions of several Antarctic meteorites. Mem. Natl Inst. Polar Res., Spec. Issue, **46**, 144–150.

MCSWEEN, H. Y. (1977): Chemical and petrographic constraints on the origin of chondrules and inclusions in carbonaceous chondrites. Geochim. Cosmochim. Acta, **41**, 1843–1860.

MCSWEEN, H. Y., FRONABARGER, A. K. and DRIESE, S. G. (1983): Ferromagnesian chondrules in carbonaceous chondrites. Chondrules and Their Origins, ed. by E. A. KING. Houston, Lunar Planet. Inst., 195–210.

PAUL, R. L. and LIPSCHUTZ, M. E. (1989): Labile trace elements in some Antarctic carbonaceous chondrites: Antarctic and Non-Antarctic meteorite comparisons. Z. Naturf., **A44**, 979–987.

PRINZ, M., WEISBERG, M. K., HAN, R. and ZOLENSKY, M. E. (1989): Type I and II chondrules in the B-7904 carbonaceous chondrite. Meteoritics, **24**, 317–318.

REUTER, K. B., WILLIAMS, D. B. and GOLDSTEIN, J. I. (1989): Determination of the Fe-Ni phase diagram below 400°C. Metall. Trans., **A20**, 719–725.

ROBIE, R. A., HEMINGWAY, B. S. and FISHER, J. R. (1979): Thermodynamic properties of minerals and related substances at 298.15 K and 1 bar (10^5 Pascals) pressure and at higher temperatures. U. S. Geol. Surv., Bull., **1452**, 456 p.

RUBIN, A. E. (1990): Kamacite and olivine in ordinary chondrites: Intergroup and intragroup relationships. Geochim. Cosmochim. Acta, **54**, 1217–1232.

SKIRIUS, C., STEELE, I. M. and SMITH, J. V. (1986): Belgica-7904: A new carbonaceous chondrite from Antarctica; minor-element chemistry of olivine. Mem. Natl Inst. Polar Res., Spec. Issue, **41**, 243–258.

TOMEOKA, K. (1990): Mineralogy and petrology of Belgica-7904: A new kind of carbonaceous chondrite from Antarctica. Proc. NIPR Symp. Antarct. Meteorites, **3**, 40–54.

TOMEOKA, K. and BUSECK, P. R. (1985): Indicators of aqueous alteration in CM carbonaceous chondrites: Microtextures of a layered mineral containing Fe, S, O and Ni. Geochim. Cosmochim. Acta, **49**, 2149–2163.

TOMEOKA, K., KOJIMA, H. and YANAI, K. (1989): Yamato-86720: A CM carbonaceous chondrite having experienced extensive aqueous alteration and thermal metamorphism. Proc. NIPR Symp. Antarct. Meteorites, **2**, 55–74.

YUND, R. A. and HALL, H. T. (1968): The miscibility gap between FeS and $Fe_{1-x}S$. Mater. Res. Bull., **3**, 779–784.

ZOLENSKY, M., BARRETT, R. and PRINZ, M. (1989): Mineralogy and petrology of Yamato-86720 and Belgica-7904. Papers Presented to the 14th Symposium on Antarctic Meteorites, June 6–8, 1989. Tokyo, Natl Inst. Polar Res., 24–26.

ZOLENSKY, M., PRINZ, M. and LIPSCHUTZ, M. (1991): Mineralogy and thermal history of Y-82162, Y-86720 and B-7904. Papers Presented to the 16th Symposium on Antarctic Meteorites, June 5–7, 1991. Tokyo, Natl Inst. Polar Res., 195–196.

(Received August 2, 1991; Revised manuscript received October 11, 1991)